Evaluation of Microscopic FRET Measurements to Analyse Protein Interactions in Human Cells

Diploma Paper
by
Jenny Pettersson
and
Mikael Sebesta

Lund Reports on Atomic Physics, LRAP-268
Lund, February 2001

Abstract

Methods based on confocal microscopy and laser spectroscopy are evaluated to investigate the technique known as Fluorescence Resonance Energy Transfer (FRET). FRET is used to detect protein interactions in human cells. Two different methods of detecting FRET are evaluated: Bleaching and Steady-state. FRET is a powerful tool for measuring interactions and distances surpassing the resolution of ordinary light microscopy but the results show that quantitative measurements are very difficult to implement.

Contents

1. Introduction

This diploma work deals with Fluorescence Resonance Energy Transfer (FRET)[1-9] to detect interactions between proteins in cells. Ten-m1[11,12] is a well-known transmembrane protein in human cells but some of its functions are still to be explained. When studying proteins and their activity an often-used approach is to find a binding partner with known properties, and by doing so, gain information about the function of the protein. To investigate if the protein and its candidate binding partner are linked they can be extracted from the cell and then further analysed with electrophoresis. However, when extracting the proteins, the bonding can be broken and it would be preferable to do the analysis in the proteins right environment. Today there is no satisfactory method of studying protein reactions inside cells but the development of different FRET techniques[3,10] has brought a promising aspirant for these types of measurements. Many groups around the world have started to use FRET in these kinds of protein measurements and this diploma work is the first step to bring the technique to the departments at Lund University. Two different techniques of measuring FRET was evaluated and ultimately used to measure if the transmembrane protein Ten-m1 interacts with a candidate protein, profilin.

FRET introduces an alternative deactivation path for an excited fluorescent molecule (donor). Instead of fluorescing, when excited, the molecule transfers its energy to a neighbouring fluorescent molecule (acceptor) with an emission spectrum matching the donor's excitation spectrum. In the presence of FRET the donor molecule will change its fluorescence properties[13] such as intensity and fluorescence lifetime. Because energy transfer occurs over distances of 10-100Å, a FRET signal corresponding to a particular location within a microscope image provides an additional magnification surpassing the optical resolution of the microscope. Light microscopy has a fundamental limit of about ~0,3 μm, which is often inadequate for many studies. Already from the beginning, with the first derivation by Förster[1], one of the most attractive features of FRET was the measurement of the relative distance between the acceptor and the donor. This is one of the principals and unique benefits of FRET for microscopic imaging[1], intimate interactions of molecules labelled with a donor and an acceptor can be seen. The strong dependence between the efficiency of FRET and the distance between the two fluorochromes have led to the often-quoted reference of FRET as a "spectroscopic ruler". With spectroscopic measurements in the microscope much of the information regarding structures and molecular interactions can be obtained. Fluorescence measurements are very sensitive and often relatively easy to perform. The result can be very difficult to quantify because of the complexity of the samples. A successful quantitative analysis of FRET depends on the availability of correct controls and on the ability to choose the best method available for carrying out the FRET measurements on particular samples.

The analysis was done using two FRET techniques: Bleaching and Steady-state[3]. Bleaching detects FRET by measuring the fluorescence intensity of the donor before and after bleaching of the acceptor fluorochrome. A Krypton-ion laser[19] tuned to 407 nm was used to excite the donor while an Argon-ion laser at 514 nm was used to bleach the acceptor molecule. When bleaching a fluorescent molecule the original optical properties of the molecule are lost as it changes its electronic energy structure through chemical reactions. The energy transferred to the acceptor will after bleaching add to the fluorescence of the donor and thus increase its fluorescing intensity.

Steady-state measurements compare the intensity from negative controls, only containing the donor, with positive control samples, carrying both donor and acceptor molecules, through matching filters. The FRET signal is then calculated using image analysis software.

This project was done in collaboration with the Department of Experimental Pathology at Lund University Hospital. Proteins were tagged with fluorescing molecules[14,15] using gene manipulation and cloning techniques[16-18]. Both Ten-m1 samples and positive controls with an amino acid chain with known length linking the donor and acceptor were produced to evaluate FRET techniques.

The laboratory work was performed at Lund University Medical Laser Centre using a confocal microscope[1,20-22] for quantitative fluorescence measurements. The confocal microscope gives the possibility to measure the fluorescence intensity in a volume element of the cell, without interactions from other parts of the cell.

In this report the concept of FRET, fluorescence molecules and the methods used to detect FRET is briefly presented. Finally, the agreement between the theory and the experimental results is given.

2. Theory

The objective of this chapter is to give an introduction to Fluorescence Resonance Energy Transfer and the methods used to detect it. It also deals with the basics of fluorescence, confocal microscopy and protein labelling.

2.1 Fluorescence

Fluorescence is probably the most important optical readout mode in biological confocal microscopy because it can be so much more sensitive and specific than absorbance or reflection. These advantages of fluorescence are critically dependent on the availability of suitable fluorochrome (fluorescing molecule) that can either be tagged onto biological macromolecules or whose optical properties are sensitive to the local environment.

Fluorescence is the spontaneous emission of light from an atom or molecule following excitation by means of for instance heating, chemical reaction or photon absorption. In this work only the last means will be considered. The definition of fluorescence requires that emission occur between electronic energy states of the same electronic spin states. Emission between states of different electronic spin is termed phosphorescence and this process in general has a much longer lifetime, 10^{-4} seconds to seconds, compared to fluorescence lifetime of 10^{-10} to 10^{-5} seconds. Fluorescence emission also has a longer wavelength and thus less energy than the incident excitation photons. This is due to energy loss caused by relaxation to the lowest vibrational level in the excited electronic state, termed internal conversion (see Fig. 2.1.1). This shift provides the means to use fluorescence spectroscopy to identify different molecules.

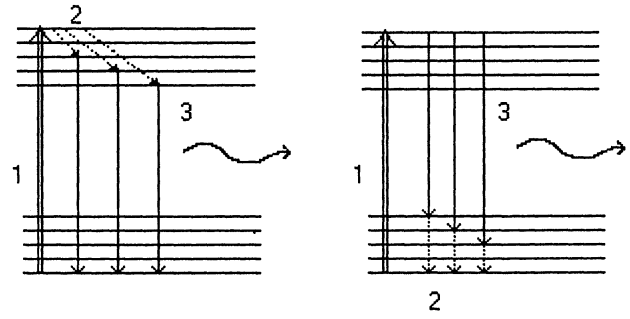

Figure 2.1.1 Energy level diagram showing the possible transitions for absorption (1) and emission (3), with internal conversion (2).

Fluorescence is of considerable diagnostic interest since it is species specific, with cross sections many orders of magnitude stronger than those for, for example, Raman scattering. There are several basic criteria that must be fulfilled to perform quantitative fluorescence measurements on a given molecule. The first one is that it has a known emission spectrum. Second, the molecule must have an absorption wavelength, which is accessible with a laser or an other light source. A third requirement is that the rate of radiative decay of the excited state is known. This is due to the fact that the fluorescence power is proportional to this rate. Another requirement is that other unwanted processes are accounted for. This involves collisional deactivation, photoionization and predissociation[13].

Additional effects that must be considered in this work of quantitative fluorescence measurements are photobleaching and saturation. Photobleaching is a process where the fluorochrome changes its fluorescence properties by a chemical reaction.

Once a fluorochrome has been excited it can decay back to its ground state by the mechanisms mentioned above. Alternatively a transition to a meta-stable state can occur. The triplet state is often long lived, allowing reactions with other molecules present, resulting in a non radiative deexcitation. Saturation is an effect that does not involve any chemical reaction, but is closely related to the excited state lifetime τ of the fluorochrome. When increasing the input laser power, more fluorochromes will be excited to a higher electron energy state. The spontaneous emission of a photon will not take place at once but will happen after an average time τ. This excited state lifetime is species specific and is between 10^{-10} and 10^{-5} seconds. When a large number of fluorochromes are in the excited state relatively fewer can be excited from the ground state and an increase in laser power will hardly increase the fluorescence output. This saturation will generate a non-linear relationship between fluorochrome concentration and input laser power, which will make quantitative fluorescence measurements difficult. Saturation thus gives another reason besides photobleaching to keep the laser power as low as possible when conducting FRET-measurements.

2.2 The principle of Fluorescence Resonance Energy Transfer

Fluorescence Resonance Energy Transfer (FRET) describes the radiation free energy transfer from excited fluorescent donor molecules (*D*) to acceptor molecules (*A*) through the near-field components of the emission and absorption dipole moments. There are a few requirements for FRET to occur:

1) The donor have a fluorescent excited state with a sufficiently long lifetime.
2) The transfer must not involve the actual resorption of light by the acceptor. Thus the fluorescent donor should be excited at wavelengths where the molar absorption of the acceptor is relatively small. This minimizes direct excitation of the acceptor and increases the amount of the acceptor probes available for energy transfer.
3) The donor molecule's fluorescence spectrum must, to some extent, overlap the excitation spectrum of the acceptor molecule. If the acceptor is an appropriate fluorescent molecule, it will fluoresce as if directly excited (Fig. 2.2.1).
4) The distance between the donor and acceptor should be small, 10-100Å. It should not be closer than ~10Å to avoid strong ground-state *D-A* interactions or transfer by exchange interactions.

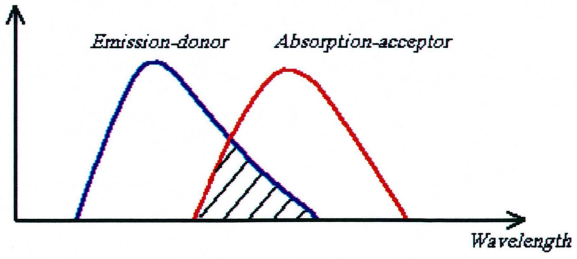

Figure 2.2.1 Overlapping donor emission and acceptor absorption spectra.

The transference dipoles of D and A must be either oriented favourably relative to each other or one (or both) must have a certain degree of rapid rotational freedom to make a dipole-dipole vectorial interaction take place. When fluorochromes are attached through molecular linkers to biomolecules in solution this condition is often satisfied.

The energy transfer process can be described as a transfer between two states:

$$(D^*, A) \xrightarrow{k_T} (D, A^*) \qquad [2.2.1]$$

where D^* and A^* denotes excited states of D and A and k_T is the rate constant of FRET between a particular D-A pair. This transfer can take place over a distance of several molecular diameters.

Förster presented the first physical theory that depicted the correct distance dependence of FRET[1]. His theory described the rate of energy transfer to be:

$$k_T = \frac{1}{\tau_D}\left(\frac{R_0}{R}\right)^6 \qquad [2.2.2]$$

where R_0 is the Förster distance, the distance between the donor and acceptor where the energy transfer is 50 percent efficient, τ_D is the fluorescence lifetime of D measured in the absence of A and R is the distance between D and A.

One thing that will complicate the interpretation of a quantitative FRET image is that the rates of deactivation from the D^* state can be differentially affected at different locations of a sample. This is due to the heterogeneous environment within biological samples. The efficiency of energy transfer, E, is a quantitative measure of a number of quanta that is transferred from D to A. It is defined as the number of quanta transferred from D to A divided with the number of quanta absorbed by D. This can also be written as in Eq. 2.2.3.

$$E = \frac{k_T}{\left(k_T + \sum_{i \neq T} k_i\right)} = \frac{k_T}{1/\tau_M} \qquad [2.2.3]$$

i refers to the different pathways of deactivation from the D^* state, τ_M is the measured lifetime of D in the presence of A, k_T is the rate constant of FRET.

The efficiency decreases as the distance between D and A increases and it can be influenced by all the different pathways through which an excited D^* molecule can be deactivated. The rates of all these pathways are independent of each other, which makes it possible to take advantage of these "extra" pathways of deactivation to determine the efficiency of FRET. This can be done by following another process quantitatively that is easier to measure than measuring FRET directly. That process does not have to involve fluorescence to be able to measure FRET efficiencies.

2.3 Orientational effects of biological samples

The orientations of the two interacting dipoles are very important for how efficient the FRET process will be. Approximative value for the orientational effect is often used in the analysis of FRET signals and is derived below[1].

The orientation factor κ^2 is considered to be the limiting factor for estimating accurate *D-A* distances from FRET data. Since the *D-A* orientations usually is not known, approximations are required. The estimates of possible orientations of *D* and *A* are determined from fluorescence anisotropy values and consequently the range of κ^2 values depend on the extent to which the *D* and *A* molecules rotate while *D* is in its excited state.

2.3.1 Interactions between two dipoles

The size of the time-dependent field strength of the near-field zone of an oscillating dipole is equal to that of a static dipole. The electric interaction between two electric dipoles, either static or time varying, is a vector dot product between the dipole moment of one dipole and the electric field of the other. κ is the factor that describes their relative orientation. Since the rate of the energy transfer, k_T, is proportional to the square of the interaction energy between *D* and *A*, $U_{D\to A}$, it is also proportional to κ^2.

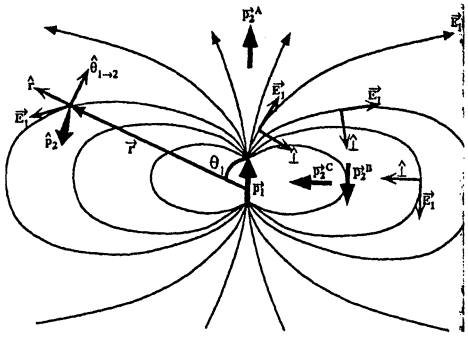

Figure 2.3.1 The field $\vec{E}_1$ of a static dipole $\vec{p}_1$ is shown. The lines run along the direction of the field. The unit vectors $\hat{\perp}$ are perpendicular to the field, where, if $\vec{p}_2$ is parallel to a $\hat{\perp}$ vector, then $\vec{E}_1 \cdot \vec{p}_2 = 0$.

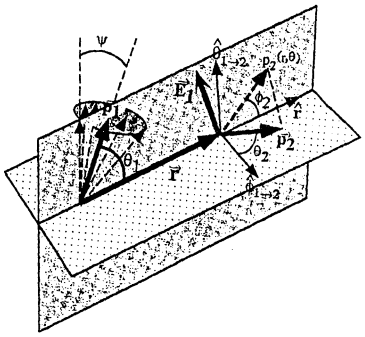

Figure 2.3.2 The coordinate systems used in the equations. The angel ψ is the angel between $\vec{p}_0$ and $\vec{p}_1$. $\left(\hat{r}, \hat{\theta}_{1\to 2}, \hat{\phi}_{1\to 2}\right)$ are explained in chapter 2.3.1.

The interaction energy $U_{\vec{p}_1\to\vec{p}_2}$ between two dipoles, $\vec{p}_1$ and $\vec{p}_2$, is a vector dot product between the electric field $\vec{E}_1$ of $\vec{p}_1$ and the moment of the other dipole $\vec{p}_2$, i.e. $U_{\vec{p}_1\to\vec{p}_2} = \vec{E}_1 \cdot \vec{p}_2$. This means that when $\vec{p}_2$ is perpendicular to $\vec{E}_1$ there will be no energy transfer regardless of how close the dipoles are (see Fig. 2.3.1).
The electrostatic field of a permanent dipole is the gradient of the equipotential surface at any point and can be expressed as follows:

$$\vec{E}_1 = \frac{|p_1|}{r^3}\left(2\cos\theta_1\hat{r} + \sin\theta_1\hat{\theta}_{1\to2}\right) \qquad [2.3.1]$$

$\left(\hat{r}, \hat{\theta}_{1\to2}, \hat{\phi}_{1\to2}\right)$ are the unit vectors of the right-hand Cartesian coordinate system, its origin at $\vec{p}_2$ and defined with reference to the displacement vector $\vec{r}$ between the dipoles and the relative orientation of $\vec{p}_1$ and $\vec{r}$ (see Fig 2.3.2).
Since k_T is proportional to $\left(U_{\vec{p}_1\to\vec{p}_2}\right)$ it is also proportional to κ^2 through:

$$k_T \propto \left(U_{\vec{p}_1\to\vec{p}_2}\right)^2 = \left(\vec{E}_1 \cdot \vec{p}_2\right)^2 = \frac{|p_1|^2|p_2|^2}{r^6}\left(2\cos\theta_1\hat{r}\cdot\hat{p}_2 + \sin\theta_1\hat{\theta}_{1\to2}\cdot\hat{p}_2\right)^2 = \frac{|p_1|^2|p_2|^2}{r^6}\kappa^2$$
$$\Rightarrow \kappa^2 = \left(2\cos\theta_1\hat{r}\cdot\hat{p}_2 + \sin\theta_1\hat{\theta}_{1\to2}\cdot\hat{p}_2\right)^2 \qquad [2.3.2]$$

where all the notations are seen in Fig 2.3.2.

If the acceptor molecule is dynamically and completely randomly oriented the orientation of this dipole is rapidly randomized within the time scale of FRET. Thus when calculating κ^2, the orientation of this dipole can be dynamically averaged at all times.

When expanding Eq. 2.3.2 it becomes:

$$\kappa^2 = \left(2\cos\theta_1\hat{r}\cdot\hat{p}_2 + \sin\theta_1\hat{\theta}_{1\to2}\cdot\hat{p}_2\right)^2 = \left(2\cos\theta_1\sin\theta_2\cos\phi_2 + \sin\theta_1\sin\theta_2\sin\phi_2\right)^2 \qquad [2.3.3]$$

If κ^2 is averaged over the rotational space of the acceptor, assuming equal probability of every orientation, it gives:

$$\left\langle\kappa^2\right\rangle_d = \frac{1}{4\pi}\int_0^{2\pi}\int_0^{\pi}\left(2\cos\theta_1\hat{r}\cdot\hat{p}_2 + \sin\theta_1\hat{\theta}_{1\to2}\cdot\hat{p}_2\right)^2\sin\theta_2 d\theta_2 d\phi_2 \qquad [2.3.4]$$

Now when the acceptor molecule is dynamically and completely randomly oriented the distribution over the angles θ_2 and ϕ_2 is assumed to be uniform at all times. This means that the integration over θ_2 and ϕ_2 is independent of the values of θ_1 and r which leads to:

$$\left\langle\kappa^2\right\rangle_d = \left(\frac{4}{3}\cos^2\theta_1 + \frac{1}{3}\sin^2\theta_1\right) = \left(\cos^2\theta_1 + \frac{1}{3}\right) \qquad [2.3.5]$$

This equation is the correct expression for calculating the effective κ^2 for the case of a dynamically averaged, randomly oriented $\hat{p}_2$ and a fixed $\hat{p}_1$.

If both *D* and *A* are dynamically, randomly oriented $\langle \kappa^2 \rangle_d^{\langle \theta_1, \phi_1 \rangle}$ equals 2/3, for derivation see Ref. 1.
This assumption that $\langle \kappa^2 \rangle_d^{\langle \theta_1, \phi_1 \rangle} = 2/3$ is often used for two reasons:

1) Sufficient orientation information is lacking, and one hopes that the relative orientations of the transition dipoles of *D* and *A* do not have a significant effect.
2) Subsequent FRET efficiency calculations and distance estimates are anyway usually greatly simplified if κ^2 is assumed to be constant for all *D-A* pairs.

Both D and A must rotate rapidly for the rigorous limit of $\langle \kappa^2 \rangle_d^{\langle \theta_1, \phi_1 \rangle} = 2/3$ to hold.
However, $\langle \kappa^2 \rangle_d^{\langle \theta_1, \phi_1 \rangle} = 2/3$ is often a reasonable approximation even if the *D* and *A* molecules do not have total orientational randomization, due to mixed spectroscopic transitions.

2.4 Different FRET techniques

The resonance energy transfer is a rather complicated process which gives rise to a change in the fluorescing properties of the participating molecules. FRET introduces an additional deactivation pathway for the excited donor molecule and influences several photophysical characteristics of both donor and acceptor molecules. In the presence of FRET:

- The fluorescence lifetime of the donor is decreased.
- The emission of the donor is quenched, i.e. the spectral characteristics is changed.
- The photobleaching rate of the donor is decreased.
- The emission of the acceptor, excited via the donor (sensitized emission), is increased.

When studying FRET in, for example, biological samples, all these characteristics have to be considered when analysing the results. A number of methods to detect FRET have been developed during the last years. The sample itself and the goal of the studies will decide which method to use in the detection of the FRET-signal on the basis of whether a quantitative measurement is preferred or not and if an imaging system will be used. The acceptor-donor pair used will also influence the choice of method depending on factors as bleaching and spectral characteristics of the molecules. A last important factor is of course the resources at hand and if all the experimental equipment is available.

The following section is a brief description of some of these methods. There are of course other equally interesting methods that are not accounted for here. This work focuses on methods that can provide a pixel by pixel quantitative measurement in an imaging system.

2.4.1 Bleaching

The FRET efficiency can be determined by comparing the fluorescence quantum efficiency in the presence and absence of functional acceptor molecules. This can be done by preparing samples with or without an acceptor. In a microscope it is also possible to selectively photobleaching the acceptor in a region of interest and to compare the fluorescence in bleached and unbleached regions. The bleaching process involves structural change of the molecules. When illuminating the sample with a high intensity laser, corresponding in wavelength to the excitation spectrum of the molecule of interest, some of the molecules will be excited to a meta-stable state where they can react with O_2. This reaction will alter the energy structure of the molecule and it will no longer have its original fluorescence characteristics. By increasing the intensity of the illuminating laser or by increasing the time of illumination virtually all the molecules in the sample can be bleached. A model of a donor and acceptor system coupled by the energy transfer is shown in figure 2.4.1. When the acceptor is bleached the rate of fluorescence of the donor, k_{DF}, is increased as the rate of FRET, k_T, is decreased.

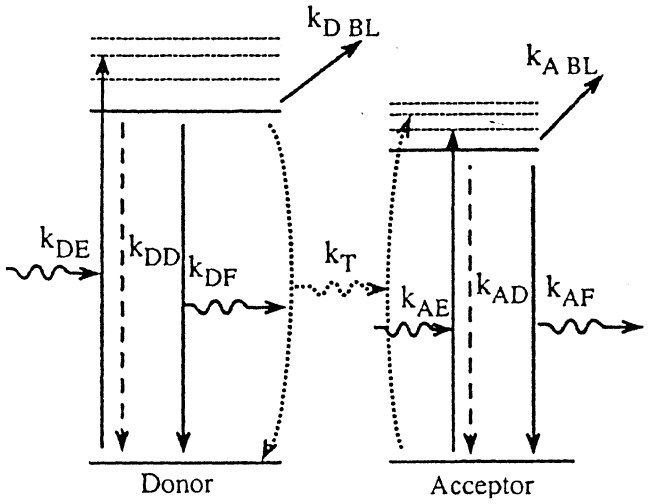

Figure 2.4.1 Donor and acceptor energy states with FRET, with the rates of excitation, deexcitation, FRET and fluorescence of the donor and the acceptor.

When bleaching the acceptor molecules the resonance energy transfer can no longer take place and the photophysical characteristics of the donor will change. The most significant change is perhaps the increase in the intensity of the donor fluorescence. Bleaching of the acceptor gives a reduced density of functional acceptor molecules and hence an increased average distance between a donor and an unbleached acceptor.
This increase can be detected by pixel by pixel comparison with the same sample before bleaching and thus provide a sensitive quantitative measurement of the rate of energy transfer.

2.4.2 Steady-state

The simplest method to observe the FRET process is to utilize Steady-state microscopy. This method requires a minimum of spectral information and is easily implemented in a fluorescence microscope.

In Steady-state FRET microscopy FRET can be detected by exciting the labelled specimen with light corresponding to the excitation spectrum of the donor and detecting light emitted at the wavelengths corresponding to the emission spectrum of either the donor and/or the acceptor. Various methods have been used for this detection but they all come down to the detection of the increase in the acceptor signal and the decrease in the donor signal in the presence of FRET. Different kinds of corrections must be made of the measured FRET-signal in order to use such signals for quantitative analysis. These corrections can involve that for cross-talk (the detection of donor signal in the acceptor emission band and vice versa) and the correction for the case when the detected signal through the filter consists of both FRET and non-FRET components.

Steady-state FRET microscopy is used with one or more of three filter sets termed Donor, FRET and Acceptor filter sets, (with either the FRET and Acceptor filter sets are the same or matched) which are designed to isolate and maximize three signals. The signals isolated are the donor fluorescence, the acceptor fluorescence due to FRET and the acceptor fluorescence due to photon excitation, respectively. The filters are chosen with respect to the donor and acceptor emission spectra and by manipulating the signals detected the FRET ratio can be calculated. This is provided that samples have been prepared that contains donor and acceptor alone and samples containing both donor and acceptor. A series of measurements of the intensities of the samples through the filter sets when the samples are excited is required to give all the values for calculation of FRET. As an example a fully compensated signal of FRET is given by:

$$FRET = \frac{F_f - D_f(F_d / D_d) - A_f(F_a / A_a)}{G * D_f * A_f} \qquad [2.4.1]$$

with the two letter symbols and their interpretation as follows:

Two-letter symbol	Filter Set	Fluorochromes present	Meaning
F_f	FRET	Donor and acceptor	The signal from a donor-acceptor specimen using the FRET filter set
D_f	Donor	Donor and acceptor	The signal from a donor-acceptor specimen using the donor filter set
F_d	FRET	Donor	The signal from a donor-only specimen using the FRET filter set
D_d	Donor	Donor	The signal from a donor-only specimen using the donor filter set
A_f	Acceptor	Donor and acceptor	The signal from a donor-acceptor specimen using the acceptor filter set
F_a	FRET	Acceptor	The signal from a acceptor-only specimen using the FRET filter set
A_a	Acceptor	Acceptor	The signal from a acceptor-only specimen using the acceptor filter set

The G factor is a compensation factor for the loss of donor emission due to FRET in the Donor filter set to the gain of the acceptor emission due to FRET in the FRET filter set. A full derivation of Eq. 2.4.1 is given in Ref. 3.

A much simpler equation is given when only two filter sets are used in the measurements. This FRET signal is corrected for cross-talk but does not separate FRET and non-FRET signals. This can on the other hand be compensated for simply by comparing the image pixel by pixel with a control specimen only containing the donor. The equation then becomes:

$$FRET = \frac{F_f - (F_d / D_d)D_f}{D_f - (D_a / F_a)F_f} \qquad [2.4.2]$$

An even more simple calculation of FRET is given by:

$$FRET = \frac{F_f}{D_f} \qquad [2.4.3]$$

This equation does not correct for either the non-FRET signal or cross-talk. However, it provides an accurate calculation of FRET when compared with other control specimens.

A quantitative pixel by pixel measurement of FRET can be made in a confocal microscope if the system is calibrated with samples with known concentrations of donor and acceptor molecules. A series of samples with different concentrations are then excited and the intensity of the emission is recorded. With the molar fluorescence coefficient through different filters the FRET rate can easily be derived from the intensities of the voxels (see chapter 2.5.2) in the sample containing both donor and acceptor. The molar fluorescence coefficient must first be measured for each fluorochrome.

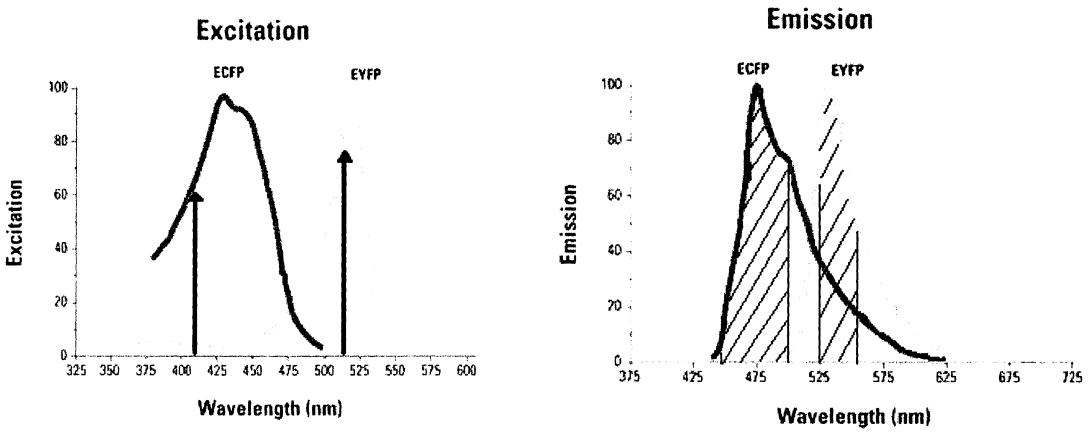

Figure 2.4.2 Excitation and emission spectra for ECFP (donor) and EYFP (acceptor) with excitation lasers (407 nm and 514 nm) and donor and acceptor filters (470/60 nm and 540/30 nm).

Other methods detect FRET not only by measuring intensities. The decrease of the fluorescence lifetime of the donor can be measured with a time-resolved system and the quenching can be measured with spectroscopy. These methods are generally much more difficult to perform and requires sophisticated equipment. The methods are beyond this diploma paper and will only be mentioned here.

2.5 Confocal microscopy

In the experiments presented below, a BioRad MRC 1024 confocal microscope was used. In this chapter the concept of confocal microscopy and what limits its performance is described.

The basic of confocal imaging is that only what is in focus is detected. The only way this is possible to achieve, is when the illumination and the detection are confined to the same spot in the specimen. This can be achieved by following the description below, see also Fig. 2.5.1 a and b. The beam is focused to an hourglass-shaped beam with an objective lens, so that the waist of the beam strikes one point at the depth of interest. The light that is reflected or fluorescing from that particular point is re-focused to a point where a pinhole aperture is placed. This only allows some of the beam to pass to the detector. Light, which originate from illuminated parts above or below the focal plane, will not be focused at the pinhole opening, which makes its contribution to the image negligible. Neither will the light that comes from other points of the same focal plane pass through the pinhole. Instead it will hit the wall of the aperture. This removes the parts that otherwise would have affected the final picture.

To create a two-dimensional image, the illuminating spot is scanned over the specimen. The scanning is often achieved with the use of vibrating mirrors. To speed up the scanning process a rotating disk can be used instead of the scanning mirrors (see Fig 2.5.1c). This disk, called a Nipkow disk, contains hundreds of pinholes arranged in a spiral, through which the light is selected. When using this disk the confocal images can be viewed directly and recorded by a photographic film or a CCD camera. In laser scanning confocal microscopy the pictures are instead saved on a computer and displayed on a monitor.

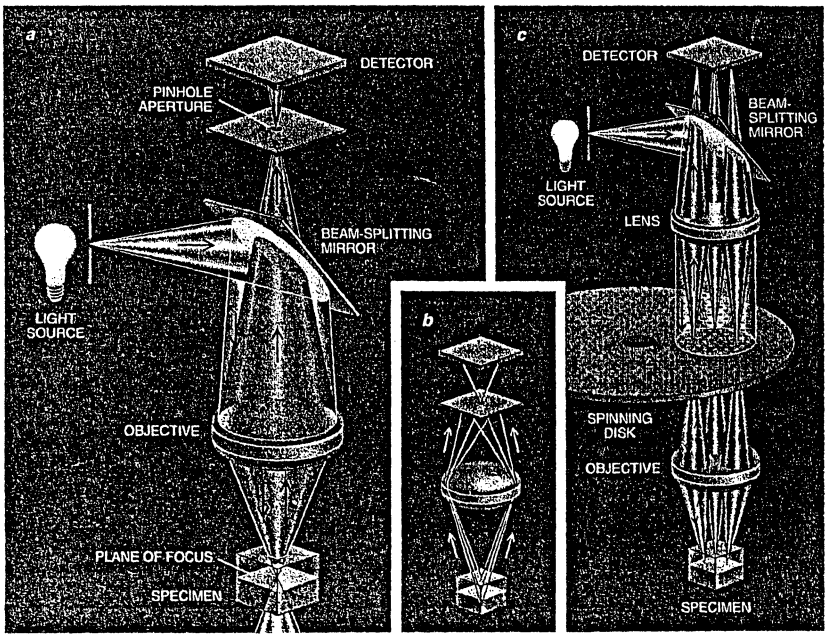

Figure 2.5.1 The principle of a confocal microscope.

2.5.1 Signal-to-noise ratio

As mentioned before, the signals of interest in confocal microscopy and particularly in FRET-measurements are often very weak. The image quality can be determined by considering the signal-to-noise ratio[20] ($R_{S/N}$) of the image, which means the level of investigated signal compared to noise from surroundings and statistical errors.

Shot-noise is the most important source of noise and it arises from the statistical variations in the number of detected photons, which obey a Poisson distribution. The Poisson distribution has the property that its mean is equal to its variance, and as the noise is given by the square root of the variance. The shot-noise of a signal containing n photons is then equal to $\sqrt{n}$. This shot-noise gives rise to the fundamental limit of $R_{S/N}$. If the only source of noise was the shot-noise, the $R_{S/N}$ would increase with an increased pinhole in the confocal microscope. However, there are other sources of noise, e.g. background, originating from autofluorescence in the specimen and the optical system, which will increase with an increasing pinhole. Consequentially the overall $R_{S/N}$ will decrease with a larger pinhole.

Increasing the laser power is not without problems either, as the power incident to the specimen is limited by effects such as radiation damage and heating of the specimen. In deciding on a proper laser power, it is also important to consider the saturation of the fluorochrome. In addition of limiting the signal detected, saturation also has the effect of giving a non-linear relationship between the concentration of the fluorochrome and the detected signal. This makes the interpretation of the data difficult. The conclusion is that, to get the highest possible $R_{S/N}$, both the laser power and the size of the pinhole must be considered.

2.5.2 Resolution

The optimal image of an object depends on various factors relating to the microscope itself, the object and the surrounding environment. When studying small organic objects such as cells, there is always a trade-off between resolution, signal-to-noise ratio and incident laser power. Studying FRET-signals makes these considerations crucial because of the low signal levels and the high resolution required.

The resolution of an optical system is not as obvious as it first may appear. The resolution can be defined in several ways. A common way is given by the Rayleigh criteria[20,23]. This states that two small point-objects are resolved if there is no interaction between the first fringe in the diffraction pattern of the two points. This means that to resolve the two objects, the minimum distance between them must be at least

$$d = \frac{1.22\lambda}{2n\sin\alpha} \qquad [2.5.1]$$

where λ is the wavelength of the light, n is the index of refraction and α is the angle created at the object by the radius of the exit pupil.

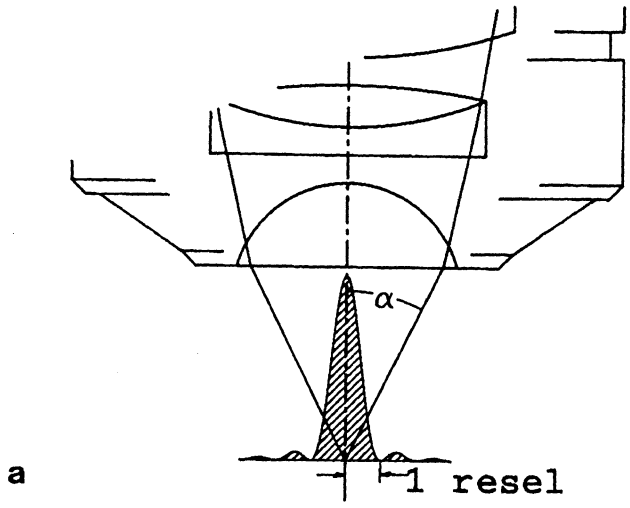

Figure 2.5.1 The geometry of the optics defining the resolution element (resel).

Since there are a few different criteria for resolution, this one should only be thought of merely as a rule of thumb, and the factor 1.22 is often ignored.
The minimum optically resolvable entity on the object is often called resel and expressed with numerical aperture it becomes:

$$1\ \text{resel} = \frac{1.22\lambda}{2NA}, \text{ with } NA = n\sin\alpha. \qquad [2.5.2]$$

Confocal microscopy has an advantage to ordinary microscopy in resolution originating from the pinhole that discriminates surrounding stray-light that would otherwise have affected the diffraction-pattern of the point source. When studying, for example, the fluorescence of an object in a confocal microscope the resel becomes slightly smaller:

$$1\ \text{resel}_{\text{conf.}} = \frac{0.8\lambda}{2NA}. \qquad [2.5.3]$$

Confocal microscopy also has a resolution element in the z-direction. This resolution is determined in the same way as the elements in the xy-direction but using the 3D diffraction image of the point source that is formed near the focal plane. Axial resolution can then be defined as the minimum distance the diffraction images of the two points can approach each other along the axis of the microscope and still be seen as two. This axial resolution is then defined as:

$$1\ \text{resel}_z = \frac{1.4\lambda n}{(NA)^2}. \qquad [2.5.4]$$

When using a confocal microscope the term voxel (Fig. 2.5.2) is often used to describe the 3D-resolution element described by the equations above.

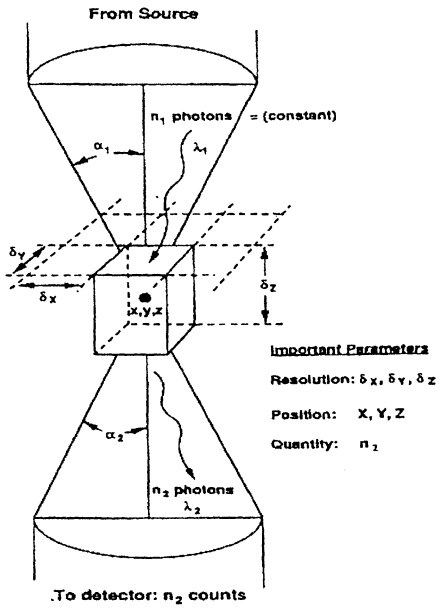

Figure 2.5.2 Voxel element in confocal microscope.

Looking at an object through a microscope one always get a pixelation of the image either in the human eye created from the discrete photoreceptors or in the pixelated image shown on a computer screen. In the confocal microscope the pixelation comes from the step size in the scanning process over the object.

It is very important to understand the difference between the size of the pixel and the size of the resel. The resel is always limited in size by the diffraction while the pixel is only limited by the mechanism scanning the object. When sampling the image information it is very important to optimise the size of the pixel to that of the resel. Nyquist's sampling theorem states that a sine wave of frequency f can only be reconstructed if samples are taken at least with a frequency of $2f$. In reality, perfect reconstruction of the original signal from the sampled data requires an ideal low-pass filter. As these are unavailable one usually use $2.3\,f$ as a minimum practical sampling frequency. This sampling theorem then extends to, that there must be at least 2.3 pixels per resel to fully appreciate the resolving power of the confocal microscope.

In reality optical features such as spherical aberrations and astigmatism also affect the resolution of the microscope. Thus it is important to understand that the resolution of an image never quite reaches the diffraction-limited resolution presented here.

2.6 Detection system - Photomultiplier

The detectors in the BioRad confocal system are PMTs. This is the most common detector type in confocal microscopy, since it is a very sensitive detector with a high internal gain. A photomultiplier (PMT)[20,23] transforms radiation to current by using a photosensitive material. Incident radiation passes through a glass window where a photocathode surface constitutes a thin layer on the inside. A photocathode is made of a photosensitive material and an electron is emitted when a photon is absorbed. The emitted electrons are then accelerated towards the first dynode by an electric field.

The signal is internally amplified by multiplication of the electrons using a chain of dynodes before reaching the anode and being detected as a current (Fig 2.6.1).

The current amplification factor (G) depends on the multiplication in each dynode (δ) and the number of dynodes (N) and can exceed 10^6.

$$G = \delta^N \qquad [2.6.1]$$

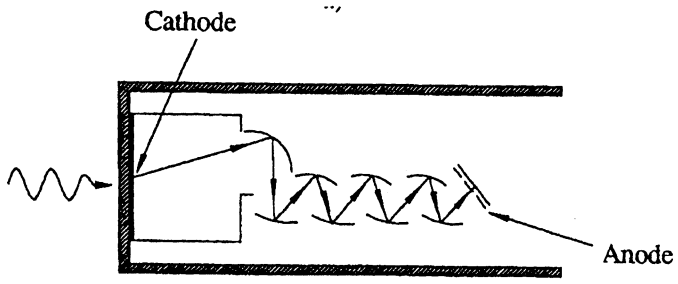

Figure 2.6.1 A common type of PMT.

2.6.1 Photon-counting

In quantitative signal registration, every photon should yield an equal part of the total signal. If the detector is based on a solid-state sensor this is usually automatically fulfilled by the sensing process (one photon corresponds to one photoelectron). Quantitative measurements using a PMT is complicated by its high internal gain yielding statistical uncertainties. However, by using the PMT in a pulse-counting mode, accurate quantitative result can be obtained also with this type of detectors. Pulse counting means that instead of measuring the time average of the current per pixel, the amount of individual output pulses is being counted. These pulses arise from the emission of individual photoelectrons from the photocathode in the PMT. By defining a threshold of the pulse size, it can be decided whether a pulse is going to be counted, or not. If the PMT output is above this threshold value, one pulse is counted. By using this discrimination method, the effect of small noise pulses generated from the dynodes of the PMT is reduced.

A major problem is when large numbers of photons are to be counted in a short time. This is because the output does not immediately return to zero. If a second pulse arrives before the first one disappears, the second, or piled-up, pulse will not be registered. Besides this problem, it is difficult counting the output when having a very high asynchronous counting rate. Ten percent of the photons are also lost because they arrive at random times.

One another important property when using a PMT is the quantum efficiency (QE). QE is defined to be the fraction of all photons absorbed by the detector that contributes to the final output signal by causing that an electron is emitted. Another issue is the noise level. This includes both dark current noise, electronic amplifier noise and multiplicative noise in the form of random variations in the actual PMT output pulses derived from identical input photons. This last type of noise is more important if the output current is measured rather than in pulse-counting mode.

QE follows the Poisson distribution. This means that if the same measurement is done repeatedly and the average result is n photons per measurement, the chance of getting the result from $n+\sqrt{n}$ to $n-\sqrt{n}$ of a specific measurement is 63%. To diminish the effect of this uncertainty, the data from many measurements can be summarized or Kalman-averaged.

QE can be as high as 30% in a PMT in the blue and green region, but this means that 70% of the photons do not contribute to the signal. To produce a photoelectron, the photon has to be absorbed in the photocathode. To improve the QE, the transmission and reflectance losses must be reduced. One way to do this is to make an angel between the incident light and the PMT to create total internal reflectance when striking the photocathode. The light that is not absorbed in the photocathode is totally reflected at the outer surface of the window and strikes the photocathode again. This continues until the light is either absorbed or it reaches the far side of the photocathode.

Manufacturers are starting to use this optical effect and are using a photocathode material having a prismatic surface made up of 45 degrees pyramids that allows a parallel, axial light beam to interact with the photocathode twice. This improves the average QE but there can be a variation in the local QE depending on where on the pyramid a photon arrives.

2.7 How to colour a protein

In the experimental part of this diploma work three different types of samples were used. The first sample contained only one of the two fluorescent proteins chosen to be able to see the FRET-signal. When only having one fluorescent protein, the samples can be used to make different background measurements. It can also be used to make controls on the fluorochromes and their reactions with for example laser light.

The second sample was used as a positive control and contained two different fluorescent proteins (FP) connected through an amino acid chain (Fig 2.8.1). When the distance between the two FP markers is small enough, there is an energy transfer and FRET-signal will be seen. This can be used to practise on the FRET-measurements and to try and see the distance dependence of the FRET-signal. One other phenomenon that may be seen is the folding of the amino acids. This gives a FRET signal despite the many amino acids in the chain that should give a long distance between the FP and result in no FRET.

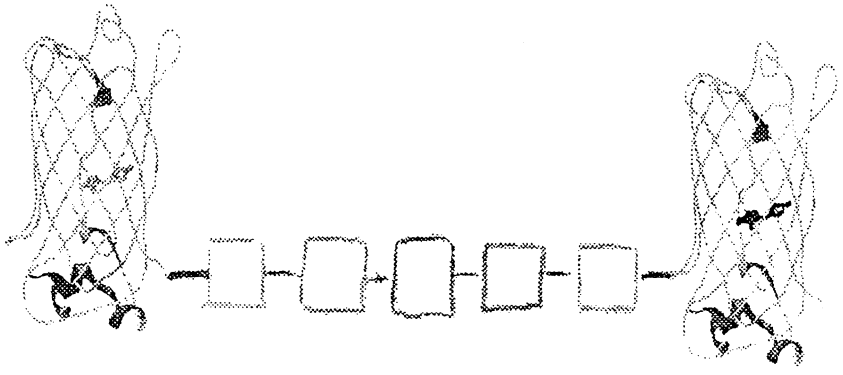

Figure 2.7.1 Fluorescent proteins linked with an amino acid chain.

The ultimate task of this diploma work has been to use the FRET method to investigate the Ten-m1 protein in human cells. The Ten-m1 protein is a transmembrane protein that connects itself to the membrane of the cell. The actual function of the Ten-m1 protein is yet to be explained and FRET measurements could give the answer. This is done by introducing different kind of proteins to the sample with Ten-m1 in hope of finding a binding partner to the Ten-m1 protein. By finding this candidate, with known use in the human cell and other binding partners, the function of the Ten-m1 may be explained. The Ten-m1 protein is marked with a FP either on the inside of the membrane or on the outside. In a similar way the candidate is marked and when connecting to the Ten-m1 protein the two FP markers are close enough to give a resonance energy transfer.

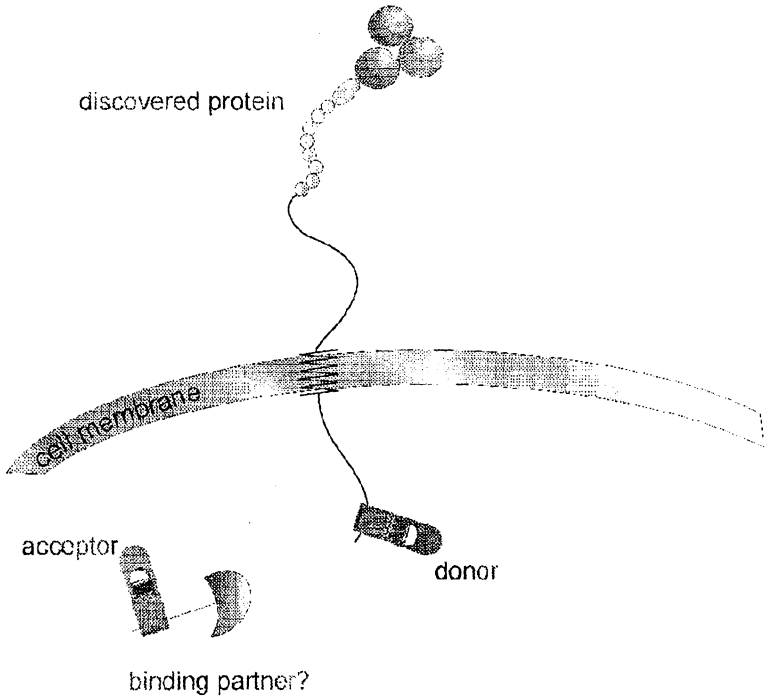

Figure 2.7.2 Ten-m1 protein and a candidate binding partner with fluorescent markers.

The actual marking of the proteins used in this study were produced at the Department of Experimental Pathology at Lund University Hospital. A full explanation of the process of producing these proteins is beyond the scope of this diploma work thus only a short description follows.

A DNA sequence coding for the FP protein is manufactured and multiplied using a variety of techniques of genetic coding. The sequence is then inserted and linked together with a plasmid vector coding for the protein of interest (Ten-m1)[16] (Fig. 2.7.3). The DNA sequence usually combines the coding of the FP with the coding for resistance to antibiotics. This combination is used in the purification of plasmid vectors so that only the specific DNA sequence of interest is extracted. This purification is done by introducing the plasmides to bacterial cells that are thereafter grown on a medium containing antibiotics. In this cloning process only the bacteria containing the DNA sequence coding for FP and resistance to antibiotics can grow. The DNA of the bacteria is then recovered and the purification is completed.

Two ways of inserting the recombinant DNA molecule into a host cell are usually used. The first method inserts the DNA by viral infection. The virus is first manipulated to contain the DNA sequence that is to be inserted. The virus enters the host cell and duplicates its DNA code to the cell.

The second method uses different kinds of chemicals, for instance Calcium Chloride (CaCl), to open the cell, so that the sequence can enter and link to the cell. After the sequence has been inserted, the cells can be multiplied through cloning to create a large sample of cells with the desired fluorescing features.

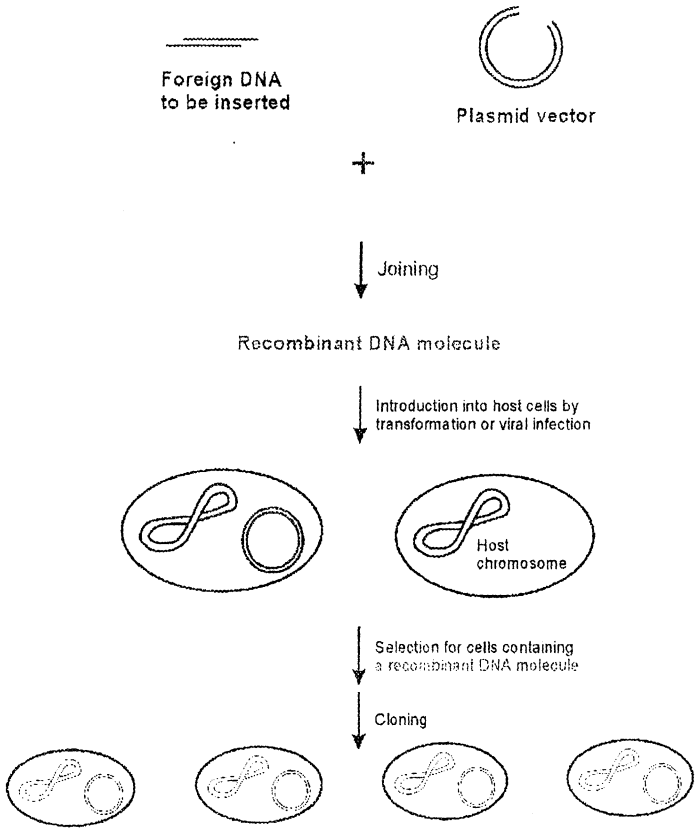

Figure 2.7.3 Insertion of foreign DNA in to host cell.

2.8 Fluorescence protein, which pair is the best?

For our study there were four different suitable fluorescent proteins to choose from, blue (Enhanced Blue Fluorescent Protein, EBFP), cyan (ECFP), green (EGFP) and yellow (EYFP). In choosing a pair, there are a few things to consider: the lasers used to excite the donor and the acceptor and the proteins spectral appearance (how much the fluorescence spectrum of the donor overlap the absorption spectrum of the acceptor and how much of the fluorescence of the donor overlap the fluorescence of the acceptor). The third thing necessary to take into account is the different filters used in front of the photomultipliers.
The lasers that best suited was the Krypton-ion (407 nm or 413 nm) and the Argon-ion (488 nm or 514 nm), while the available filters were 470/60 nm and 540/30 nm.
The spectra of the fluorescent proteins can be seen in Fig 2.8.1.

Below, we are discussing all possible combinations of donor-acceptor for our FRET study.

EBFP and ECFP

To excite the donor (EBFP) the best wavelength to use is 407 nm. At that wavelength the normalized absorbance is ~60%, which is good. One disadvantage is that the normalized absorbance of the acceptor (ECFP) is as high as ~60% at that wavelength. The fluorescence spectrum of the donor overlaps the absorbance spectrum of the acceptor almost completely. For bleaching the acceptor with the laser with λ=488 nm, there is only an absorbance of ~8%, which is not sufficient. It is even worse at λ=514. This pair is not good because of the high absorbance of the acceptor at λ=407 nm and the low absorbance of the acceptor at λ=488 nm.

EBFP and EGFP

To excite the donor (EBFP) the best wavelength to use is 407 nm, as written above. The normalized absorbance of the acceptor (EGFP) is ~16% at that wavelength. The fluorescence spectrum of the donor overlap the absorbance spectrum of the acceptor quite well. If the acceptor is to be bleached, the laser with the wavelength of 488 nm is suitable, the normalized absorbance is ~90% at 488 nm, which is very good. One positive thing is that the donor is not excited at 488 nm.

EBFP and EYFP

To excite the donor (EBFP) the best wavelength to use is 407 nm, as described above. The absorbance of the acceptor (EYFP) is ~5% at that wavelength, which is good. The fluorescence spectrum of the donor overlap some of the absorbance spectrum of the acceptor. Bleaching is best done with λ=514 nm, where the absorbance of the acceptor is ~70% and there is no absorbance of the donor.

ECFP and EGFP

To excite the donor (ECFP) the best wavelength to use is 407 nm. At that wavelength the normalized absorbance is ~60%, as indicated above. The normalized absorbance of the acceptor (EGFP) is ~16% at that wavelength. The fluorescence spectrum of the donor overlap the absorbance spectrum of the acceptor quite well. If the acceptor is to be bleached, a laser wavelength of 488 nm is preferable, as the normalized absorbance is ~90% at this wavelength. The donor absorbs almost nothing at this wavelength.

ECFP and EYFP

To excite the donor (ECFP) the best wavelength to use is 407 nm, as described above. The absorbance of the acceptor (EYFP) is ~5% at that wavelength, which is very good. More then half of the fluorescence spectrum of the donor overlap the absorbance spectrum of the acceptor. Bleaching is best done with λ=514 nm as the absorbance of the acceptor is ~70% and there is no exciting of the donor at this wavelength.

EGFP and EYFP

To excite the donor (EGFP) the best wavelength to use is 488 nm. At that wavelength the normalized absorbance is ~90%, which yields a very efficient excitation. On the other hand the absorbance of the acceptor (EYFP) is ~35% at that wavelength. The fluorescence spectrum of the donor overlap the absorbance spectrum of the acceptor almost completely. Bleaching is best done with λ=514 nm where the absorbance of the acceptor is ~70%. However, at this wavelength the absorbance of the donor is ~50%, which makes this combination unusable for FRET studies.

Discussion

The three best pairs are thus EBFP & EYFP, ECFP & EGFP and ECFP & EYFP. To decide which pair to use, the available filters in front of the PMTs have to be taken into consideration. The two best suited filters are bandpass filters, 470/60 nm and 540/30 nm. The donor fluorescence should thus overlap the 470/60 nm filter and the emission of the acceptor the 540/30 nm filter.

When using EBFP & EYFP, one can see in Fig 2.9.1 that only half of the fluorescence of the EBFP is transmitted through the 470/60 nm filter, while the fluorescence of the EYFP matches the 540/30 nm filter quite nicely.

With ECFP & EGFP, the peak of the fluorescence spectrum of the ECFP matches the filter 470/60 nm, but the fluorescence of the EGFP does no overlap the filter 540/30 nm very well.

The pair ECFP & EYFP and their fluorescence matches both filters perfectly.
Thus the conclusion is that ECFP & EYFP is the best protein pair to use in the experiments in this diploma work.

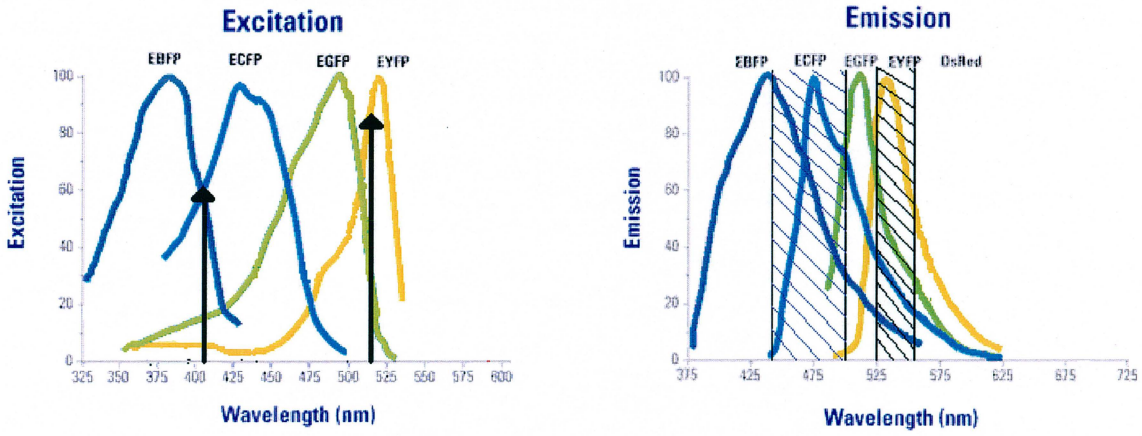

Figure 2.8.1 The excitation spectra for the different fluorescent proteins with used lasers and the emission spectra for the different fluorescent proteins with used filters.

3. Materials and methods

At the Department of Physics at Lund Institute of Technology, a system for confocal microscopy is used in research. This confocal microscope was very suitable for the purpose of this diploma work and gave an opportunity to make quantitative measurements of FRET. For the bleaching processes another laser than the lasers already inserted into the system, was needed to suit the excitation spectrum of the yellow fluorescent protein. This was found to be an Argon-ion laser positioned in a room above the microscope room. Thus the first part of the diploma work was to lead the beam down to the microscope and to find the most suitable entrance to the filter box. To be able to do all the experiments it was a necessity to have both negative and positive controls and of course the samples with both Ten-m1 and the candidate protein profilin. These samples were all made by the Department of Experimental Pathology at Lund University Hospital.

3.1 System

Below, the confocal fluorescence microscope system used in the studies is described. This system can be divided in several subunits, each presented in a specific paragraph in this section.

3.1.1 Lasers

There were four different lasers that could be used with the microscope: a Krypton-ion laser (λ=407nm and 413nm), a modelocked Titanium-Sapphire laser (λ=just below 800 nm), a Helium-Neon laser (λ=633 nm) and an Argon-ion laser (λ=488 nm and λ=514 nm). The Titanium-Sapphire laser is very good to use for two-photon microscopy, but since only one-photon excitation was used in these experiments this laser was not considered. The Krypton-ion (407 nm) and Argon-ion (514 nm) lasers were chosen to match the excitation curve of the fluorochromes, as described above. As discussed before the best fluorescent protein pair for the experiment was ECFP and EYFP. Since these give the best results with the Krypton-ion laser with λ=407 nm and the Argon-ion laser with λ=514 nm, these were the lasers and the wavelengths that were used.

3.1.2 Filter Box

The filter box in front of the microscope is designed for simultaneous use of three different lasers, a Helium-Neon laser, a Krypton-ion laser and a Titanium-Sapphire laser. Each laser has a separate entrance to the box. Thus, all three lasers can be used at the same time. Inside the box there are filters, dichroic mirrors and safety shutters to optimize the use. In the experiments another laser was used instead of the Helium-Neon (He-Ne) laser, namely the Argon-ion laser. To be able to get it into the filter box the He-Ne laser was removed and its entrance was used. An overview of the filter box can be seen in Fig 3.1.1.

Entrance 1 was used for the Krypton-ion laser. Inside this entrance there is a dichroic mirror (4) reflecting or transmitting the beam into two different paths, depending on the laser wavelength. In this path another dichroic mirror (5) is placed. This is used to align the He-Ne laser beam that comes through entrance 2.

The reflected path, for wavelengths below 400 nm, contains optics compensating for the achromatic properties of the objective lens in the UV region. In this study the non-correcting transmission path was used. Because this mirror is chosen for the He-Ne laser it is not optimal for the Argon-ion laser. Most of that wavelength is transmitted instead of reflected in the right direction. A high input power of this laser was thus required. One other reason for the higher power was the long distance from the laser source to the microscope. The laser was standing in a room above the microscope and the beam had to be led down through a hole in the ceiling with the help of seven different mirrors. This long distance resulted in losses in laser intensity. After this there is a mirror (6) to change the direction of the laser into two filter wheels (7). The first one contains wavelength selective filters. This makes it possible to select which laser beam that should enter the microscope. The other one contains different grey filters, allowing easy adjustable laser power at the specimen. Then there is a dichroic mirror (8) used to again co-linearly align the two laser beams splitted by dichroic mirror (4). Next there is a safety block (9) that only let light through when the lid is on and the scanning button is activated on the computer. The last optical component in the filter box is a dichroic mirror (10). This mirror reflects the beams that enters at 1 and 2 and transmits the light from entrance 3, the part for the Titanium-Sapphire laser beam. From here the laser light enters the scanning box of the confocal microscope.

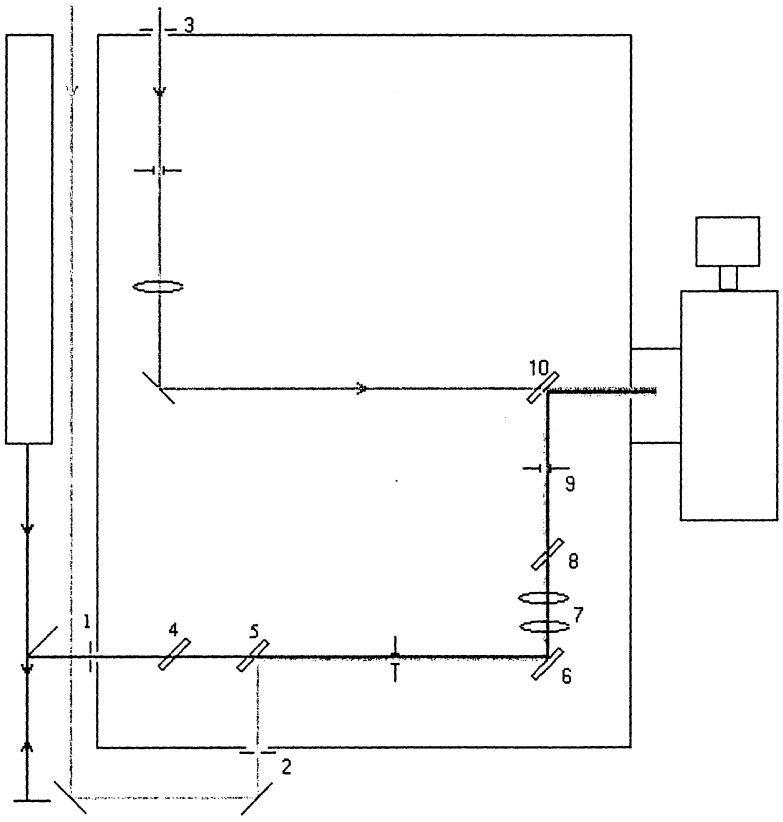

Figure 3.1.1 The filter box.

3.1.3 Mirrors

Before entering the filter box the laser light is directed with the help of mirrors. The mirrors are also used to align the laser beams so that they perfectly hit the specimen in the microscope. The rough alignment is done with the help of two apertures; one outside the filter box just in front of both the entrances and one before the laser beam leave the filter box into the microscope. The fine alignment is performed using a pinhole and a prism with a ring marked on it, positioned in the scanning box. When the alignment is done perfectly, the laser beam should hit right in the centre of the ring.

3.1.4 Scanning box

The main part of the system is the MRC 1024 scanning box. The optical arrangements of this can be seen in Fig. 3.2.2. Two scanning mirrors in this box scan the laser beam to allow image acquisition. The remitted light from the specimen is descanned by the same mirrors, and is led to three independent photomultiplier tubes (PMT). These detectors make it possible to simultaneous record images in three colours and display them with a single monitor for image display and user interface. These PMTs have enhanced sensitivity. Digital filtering is used to optimize the signal-to-noise ratio for all scan conditions. There is also a fast photon counting mode with automatic set-up, which allows quantification and acquisition of high quality, full brightness images from extremely low signal intensities.

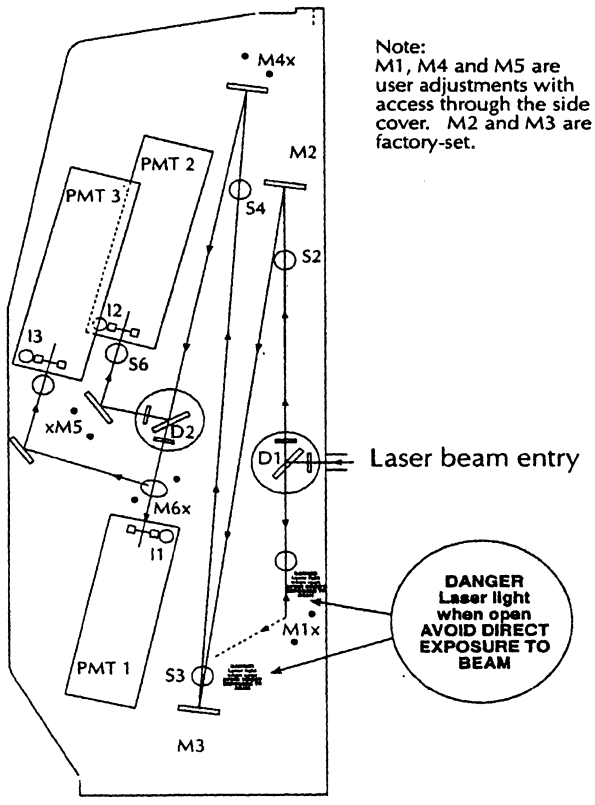

Figure 3.1.2 The scanning box in the microscope system.

There are also three different dichroic mirrors. Two of these mirrors are interchangeable and different combinations can be chosen to control what wavelengths to detect by the different PMTs to get as much information as possible from the signal.

- D1 decides what wavelengths to transmit into the system.
- D2 splits the beam, one part goes directly to PMT2, and the other one goes to M6x.
- M6x is a fixed dichroic mirror which transmit all wavelengths below λ=640 to PMT1 and reflects all λ>640 to PMT3.

The different dichroic mirrors to choose from are:

Dichroic mirror	**Reflectance (R)**
B1	20%
T1	488nm, 568 nm, 647 nm (10 nm bandwidth)
TS1	670 nm - 1000 nm
IN1	330 nm - 370 nm
IN2	< 440 nm, > 680 nm
E2	< 560 nm
T2A	500 nm - 550 nm
TS2	> 640 nm

If the dichroic mirror is positioned at D1, R means it goes to the microscope, the rest of the light goes to the PMT system. If it is positioned at D2, R means light reflected towards PMT2, while other wavelengths are transmitted towards PMT1 and PMT3. To be able to choose even more precisely what wavelengths to detect there is a filter in front of every PMT. These filters are either high-pass, low-pass or band-pass with a width of 30 nm-60 nm.

To help choose what dichroic mirrors and filters to use, for a specific measurement, a computer program written by Tommy Sjögren was employed. This program includes all reflection/transmission profiles of the filters and dichroic mirrors that are used in the microscope. Tommy has done a Matlab code that multiplies the chosen filters and dichroic mirrors. It then creates the images of the spectral percentage of the fluorescence that will reach the different PMTs. This simplifies the use of the microscope very much. An example of the image from Tommy's program is shown in Fig 3.1.3.

The program suggested that the best dichroic mirrors for Steady-state measurements were IN2 as D1 and E2 as D2. These reflect and transmit the right wavelengths in the best way among the available dichroic mirrors. For the Bleaching measurements the same dichroic mirrors were used in the image acquisition mode. When bleaching the cells with the Argon-ion laser for 15 minutes, the IN2 was changed to T2A on the D1 position. This was the best alternative, because it reflects $\cong$ 95% of the laser light to the sample, increasing the effectivity of the bleaching.

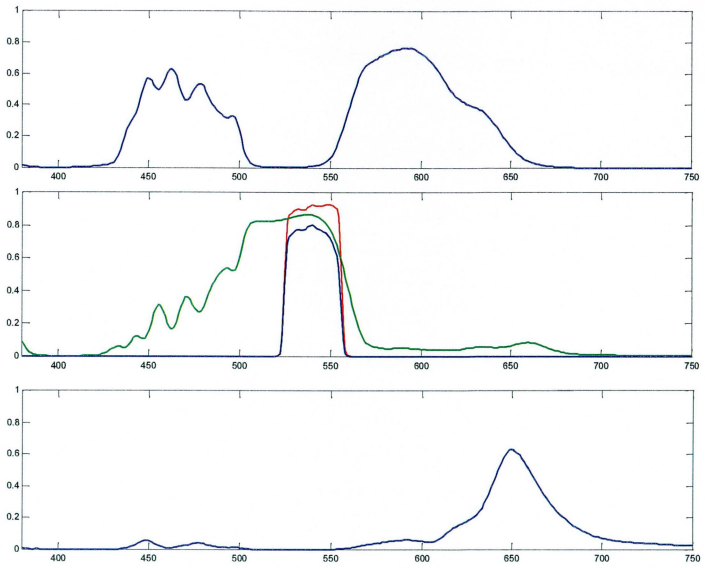

Figure 3.1.3 A result image from Tommy's program when using IN2 as D1, T2A as D2 and the 540/30 nm filter in front of PMT2. The blue line in the signal displayed on the different PMTs, the green line is the result without the filter, which is seen as the red line.

When choosing which cell to measure on, the microscope was not used in its confocal mode. Instead it was used as an ordinary microscope with a mercury lamp as a light source. The confocal mode was only used when performing the measurements. In this mode, the selection of filters in front of the PMTs and in the filter box were made through the computer interface. In the acquisition program parameters could be controlled such as zooming, which mode the PMT should have and how the accumulations should be added (Kalman filtering, Accumulate etc.).

The dichroic mirrors in the microscope, discussed above, can be changed by hand and are not adjustable through the computer. The changing of the focus on the microscope was also done by hand. There were also four objectives with different magnifications to choose from. The one used in the measurements was the oil immersion objective with magnification x40 and NA=1,3.

It is also possible to use ultra short pulses and to connect a spectrometer to the system. The later can be used to record the full fluorescence emission spectrum in just one pixel.

3.2 Samples

As mentioned before the samples were prepared at the Department of Experimental Pathology at Lund University Hospital. The positive controls had different number of amino acids (aa) between the two fluorescent proteins. The lengths studied were 6aa, 10aa, 14aa, 17aa, 18aa, 22aa and 30aa. It is very difficult to produce these samples and it was not possible to make any smaller than 6aa or to make all distances in between these values. For the background measurements, there were also negative controls consisting of cells produced with only one of the fluorescing proteins, ECFP or EYFP, as well as samples with cells with only Ten-m1 marked with ECFP and only profilin marked with EYFP. To make the final control if the Ten-m1 reacted with profilin there were samples with both of them marked with the same fluorescent protein as in the negative control samples.

3.3 Measurements

Both Bleaching measurements and Steady-state measurements were performed. The measurements were divided into three parts: negative controls, positive controls and Ten-m1. All experimental work was done during the time when the lab and the lasers were accessible.

Starting with the Bleaching measurements, the time of exposure with the 514 nm laser to bleach the EYFP fluorochromes was established by measurements on negative controls containing only EYFP. Varying the power and the time of exposure of the samples gave the approximate time of 7 minutes at a power of 500mW to bleach the EYFP to the point where no longer any intensity was observed through the 540/30 nm filter. The dichroid used when accumulating the images was also changed to one that reflected almost 100 % of the power onto the sample. Because of the variations in concentration of EYFP between different cells, a bleaching time of 15 minutes was set for further measurements. To determine if the 514 nm laser effected the ECFP fluorochrome, the same measurement was repeated for samples containing only ECFP.

When measuring on the positive controls, an image of a cell was initially accumulated through the 470/60 nm filter excited by the 407 nm laser. Part of the cell was then bleached while the other part was kept unbleached for reference purpose. This was possible by zooming in on the part to be bleached and thus when changing laser only illuminating the area visible in the confocal microscope. After 15 minutes the dichroid and the laser was changed back to accumulate an image through the 470/60 nm filter after zooming out to the original magnification.

The Steady-state measurements were conducted using 407 nm light for excitation. The fluorescence intensities for non-FRET cases were first measured through the two detection filters. Both negative and positive controls were used in the same way to establish these non-FRET signals. To measure FRET signals, images of a cell were first accumulated through the 470/60 nm filter. The filter was then changed to 540/30 nm, to detect the intensity in the yellow spectrum.

3.4 Data analysis

When analysing the data collected from the measurements, great help was provided from Clemens Kaminsky. In his earlier studies of FRET, he used Research Systems IDL software to analyse data. IDL is software well suited for data analysis and visualization. In this software, the user works in a language much like C++. The raw data was provided from the microscope in .PIC format and was initially converted to .GIF format for easier presentation. Clemens Kaminsky already did much of the coding and only small additions were necessary for the purposes of this diploma work. The FRET analysis computer code used is given in Appendix.

When analysing the data, considerations had to be made to the different limitations in the microscope and the errors arising from the fluctuations in laser intensity.

In both the Steady-state and Bleaching measurements, the goal was to analyse the FRET signals in such a way that sources of error were eliminated through a pixel by pixel division of images of the same cell. Much effort was spent in collecting results from many samples to get good statistics of both negative and positive controls.

The analysis of the Steady-state measurements was based on recorded images of the same cell excited by the 407 nm laser and detecting the emission through two different filters matching the ECFP and EYFP emission spectrum, respectively. Three images were acquired for each cell to compensate for fluctuations in the laser intensity.

The images were then smoothed in the IDL software with a smooth factor of 2. This means that every pixel in the image was averaged in its intensity with its 8 surrounding pixels. This smoothing was performed to compensate for intensity variations in pixels, due to instabilities in the set-up. The intensity images through the two different filters of the cell were then divided, pixel by pixel, to get the FRET value (see Eq. 2.4.3). The FRET value was calculated for all the pixels in the images that were not saturated and had a value above a predefined threshold (noise elimination). An image of the cell was calculated in the IDL software to visualize the FRET value and an average value over the entire cell was then used in our analysis. This analysis was done for both negative controls only containing the ECFP and positive controls with different lengths in the amino acid chain. The negative controls provided values obtained for non-FRET samples. The highest value obtained was then used as a threshold for the FRET signal. Over 100 images of negative control cells were analysed for this purpose.

The analysis of the Bleaching measurements was based on three images of the same cell. Each cell was initially excited with the 407 nm laser to obtain a before-bleaching image through the 470/60 nm filter. Approximately half the cell was then bleached during 15 minutes using the 514 nm laser and an image was then accumulated with the 514 nm laser through the 540/30 nm filter to get a measurement of how much of the EYFP that had been bleached. Another image of the cell was then accumulated through the 470/60 nm filter, when excited with the 407 nm laser, to obtain an after-bleaching image. In the IDL software, the image before and after bleaching went through the same procedure of smoothing and thresholding as in the Steady-state measurements before the pixel by pixel division of the images. The division provides a Bleaching value of how much the signal through the blue filter has increased when the EYFP in the cell was bleached. Because of the intensity variations between different accumulated images, due to poor alignment of the laser, the Bleaching value could not be used in the analysis. The image of the Bleaching value calculated by the IDL software was because of this further analysed by choosing an area in the unbleached region as well as in the bleached region. The average pixel intensity was then calculated for each area and the division of the bleached pixel intensity with the unbleached gave a new Bleaching value, compensated for this intensity variation. The analysis was performed for negative control cells containing only ECFP and EYFP, respectively, and for positive controls with different lengths in the amino acid chains.

4. Results

The results presented in this chapter were obtained by analysing the acquired images using the IDL software. From the information in the images conclusions could be made about what had happened in the cells. Therefore it has been necessary to consult persons with knowledge about the functions and reactions in cells.

4.1 Bleaching

Fig. 4.1.1 show results obtained from a negative EYFP control. In the upper left square (frame 1) the cell through the 540/30 nm filter excited with 514 nm laser before bleaching, is displayed. After 15 minutes of bleaching of the right half of the cell, all the yellow fluorescent proteins were bleached. This is shown in the upper right square (frame 2). To make this even more clear the ratio of these two images was calculated and displayed in the lower right square (frame 4). Here it can be noticed that any scattered light does not affect the half of the cell that has not been exposed to the bleaching. The intensity difference between frame 1 and frame 2 is due to an alignment error in the microscope system.

The same method was used in fig 4.1.2, which shows another negative control, a cell containing only ECFP. Frame 1 shows an image of the cell before bleaching taken through the 470/60 nm filter excited using 407 nm laser excitation. Frame 2 shows the similar image of same cell after 15 minutes of illumination with the 514 nm laser. The division of the two frames was calculated and displayed in frame 4. This time the lower half of the cell was bleached and it is clearly seen that the 514 nm laser does not affect the blue fluorochrome.

Fig 4.1.3 shows the bleaching of a positive control with the distance 6 amino acids (6aa) between the two fluorochromes. In frame 1 a picture is displayed of the cell taken through the 470/60 nm filter excited with the 407 nm laser before bleaching. Frame 2 shows a similar image of the same cell after bleaching of the lower half of the cell. Here an intensity increase, in the half of the cell that has been bleached, can be discerned. This is more easily seen in the lower left square (frame 3) and in frame 4. Frame 3 displays the cell through the 540/30 nm filter excited with the 514 nm laser after bleaching. Frame 4 shows the division of frame 1 with frame 2 where it is clearly seen that the area where the EYFP has been bleached has an increase in the intensity through the 470/60 nm filter excited with the 407 nm laser.

A great number of measurements were performed in the same way with all the positive controls with different lengths on the amino acid chain. The results from these are shown in diagrams 4.1.1-4.1.7. Here the Bleaching value is presented for a number of measurements within the same amino acid sequence in every diagram. It appears that there is an increase in the intensity through the 470/60 nm filter with the excitation source 407 nm laser after the bleaching process. The same bleaching procedure was done on the Ten-m1 sample. Fig 4.1.4 shows the result displayed in the same way as in Fig. 4.1.3. A more detailed discussion of the results will be found in chapter 5.2.

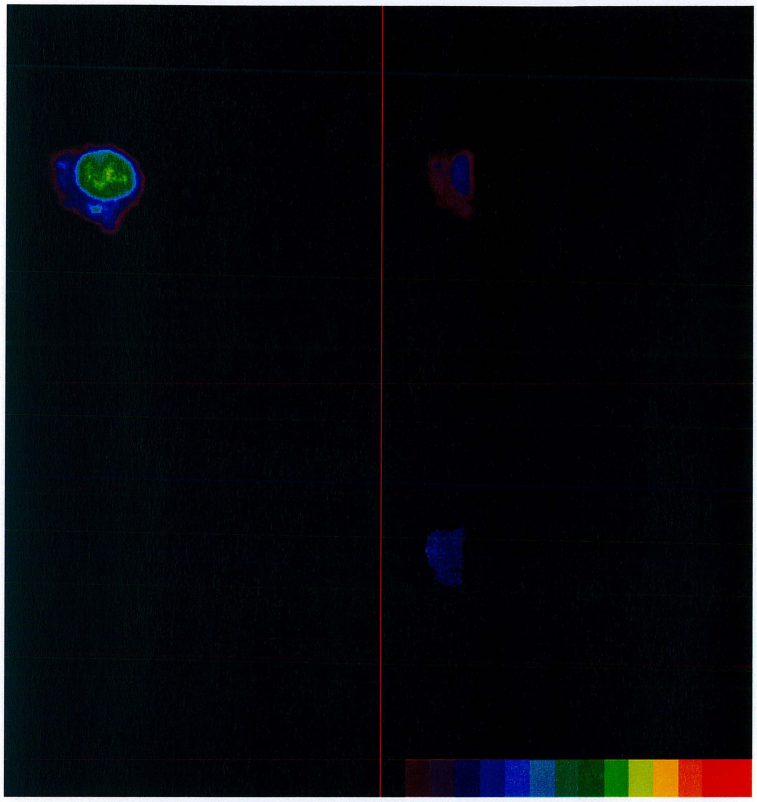

Figure 4.1.1 Bleaching of a negative EYFP control.

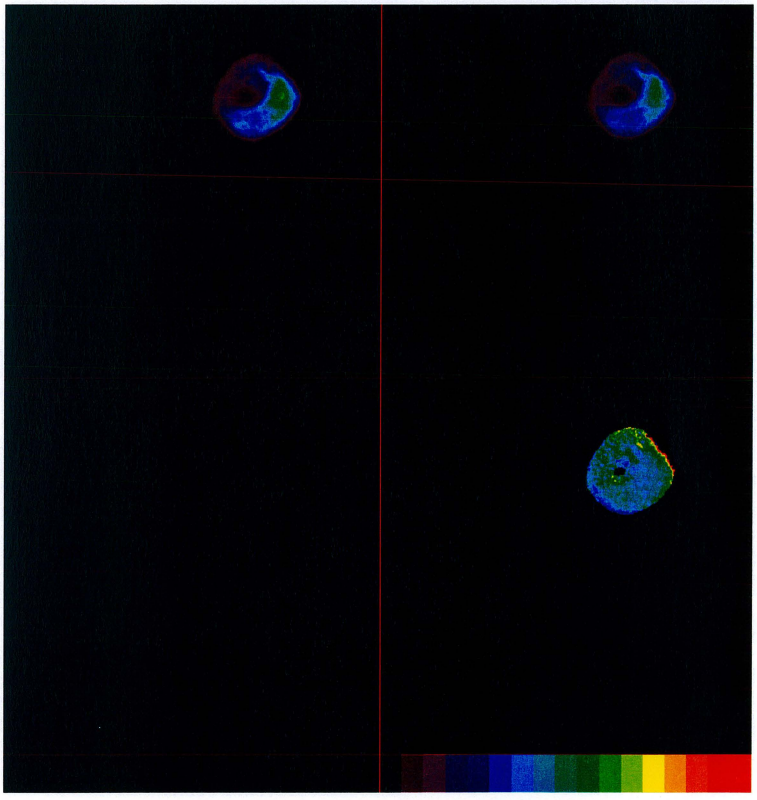

Figure 4.1.2 Bleaching of a negative ECFP control.

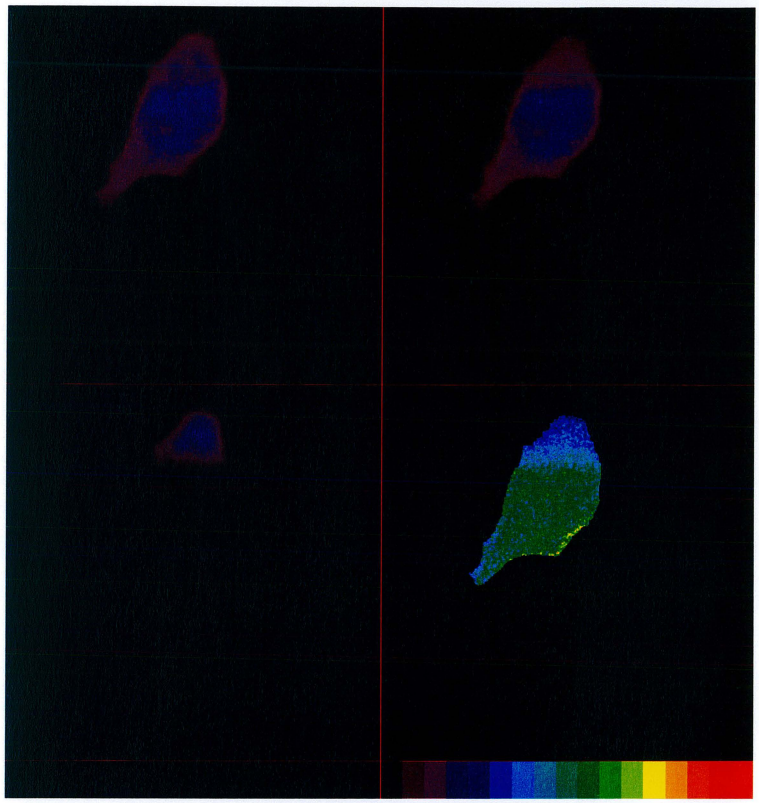

Figure 4.1.3 Bleaching of a positive control, 6aa.

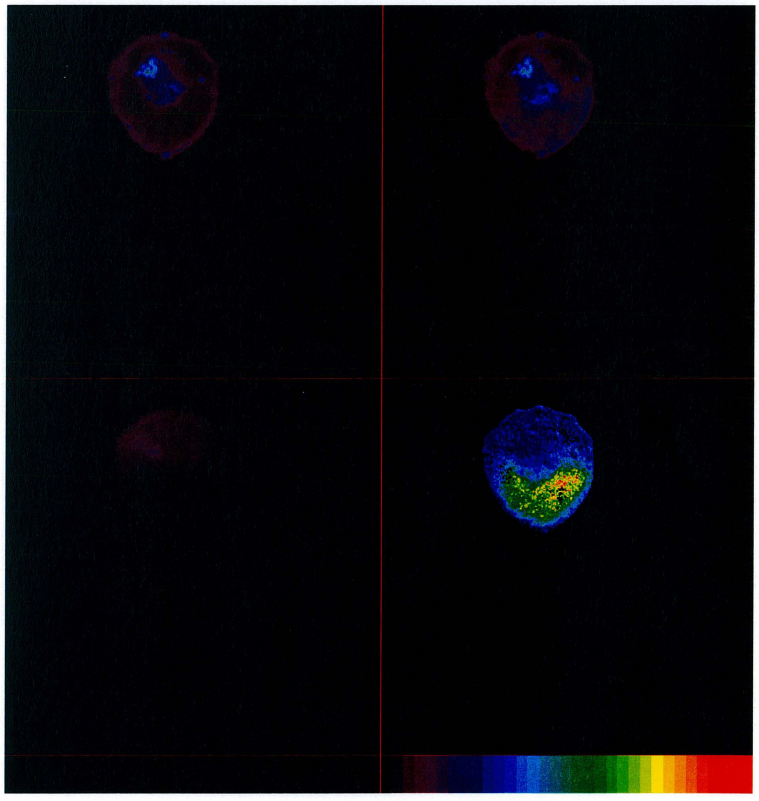

Figure 4.1.4 Bleaching of Ten-m1.

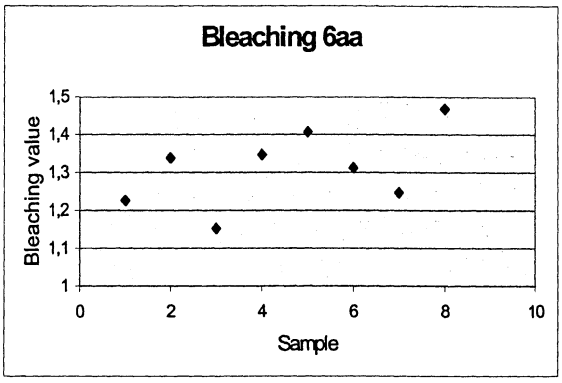

Diagram 4.1.1 Positive control 6aa

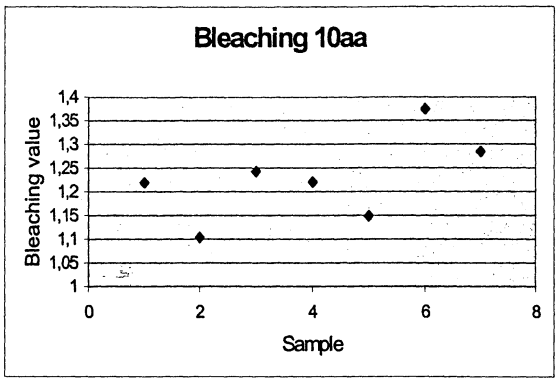

Diagram 4.1.2 Positive control 10aa

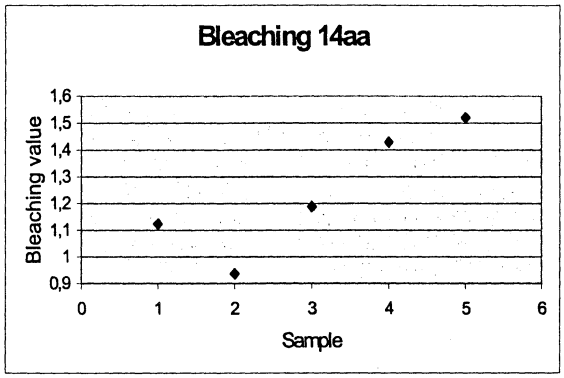

Diagram 4.1.3 Positive control 14aa

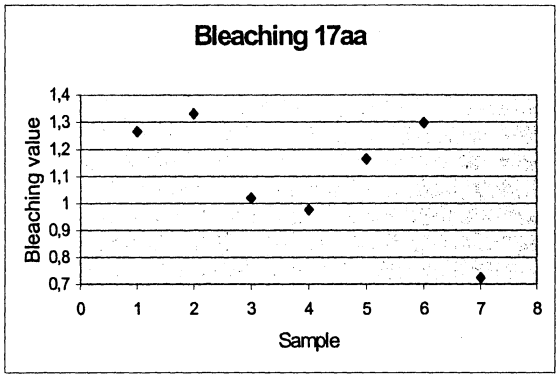

Diagram 4.1.4 Positive control 17aa

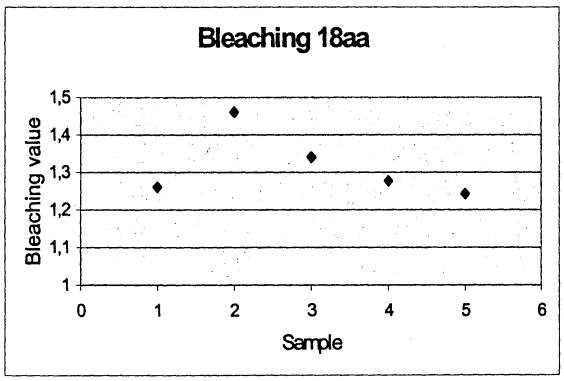

Diagram 4.1.5 Positive control 18aa

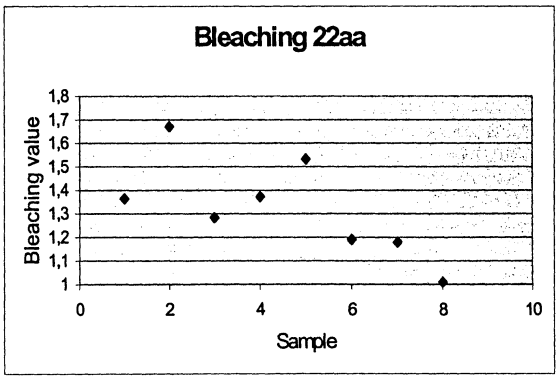

Diagram 4.1.6 Positive control 22aa

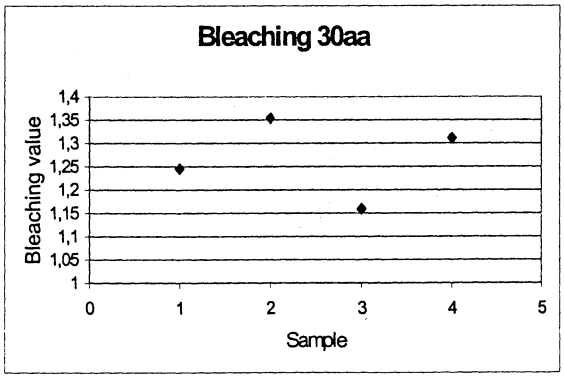

Diagram 4.1.7 Positive control 30aa

4.2 Steady-state

Fig 4.2.1 shows an acquisition of a negative control cell containing only the fluorescent protein ECFP. In frame 1 the cell can be seen through the 470/60 nm filter excited with the 407 nm laser. After change of filter another accumulation was made through the 540/30 nm filter using the same laser, frame 2. The ratio of the detected intensity between frame 1 and frame 2 was displayed in frame 4. This illustrates the background level for a FRET measurement, i.e. how much of the fluorescence of ECFP will be detected through the 540/30 nm filter. In frame 3 values used or calculated by the software for a number of parameters are displayed. The most interesting information in this frame is the value called ave_FRET. This is the mean value of the ratio within the cell (FRET value). By performing many measurements on negative control cells, the background intensity has been obtained. This is presented in diagram 4.2.1, showing the number of cells with the FRET values in the negative controls within different intervals.

A recording of a positive control is shown in Fig. 4.2.2. In this figure it can be seen that the intensities in frame 1 and frame 2 were about the same, i.e. the intensity through the 470/60 nm filter 540/30 nm filter, respectively. It is also seen in frame 3 and frame 4 that the calculated mean value of the FRET value was higher for the positive control than for the negative control.

A compilation of the FRET values obtained within different interval and for different lengths of the amino acid chains is displayed in diagram 4.2.2-4.2.8.

In diagram 4.2.9 all the FRET values are displayed by the length of the amino acid chain. To see the dependence of the length of the amino acid chain to the FRET value the mean values are shown in diagram 4.2.10. In diagram 4.2.11 the 95% confidence interval has been calculated for the mean FRET values.

Finally, an image of a Ten-m1 sample is shown in Fig. 4.2.3. In frame 1 the intensity through the 470/60 nm filter was displayed. The ECFP marked Ten-m1 is seen localised at the membrane, which was expected. Frame 2 shows the same area seen through 540/30 nm filter and the division between these two is displayed in frame 4. The result in frame 3 shows the mean value of the division between frame 1 and frame 2. In this recording, this value was well above the values of the negative controls.

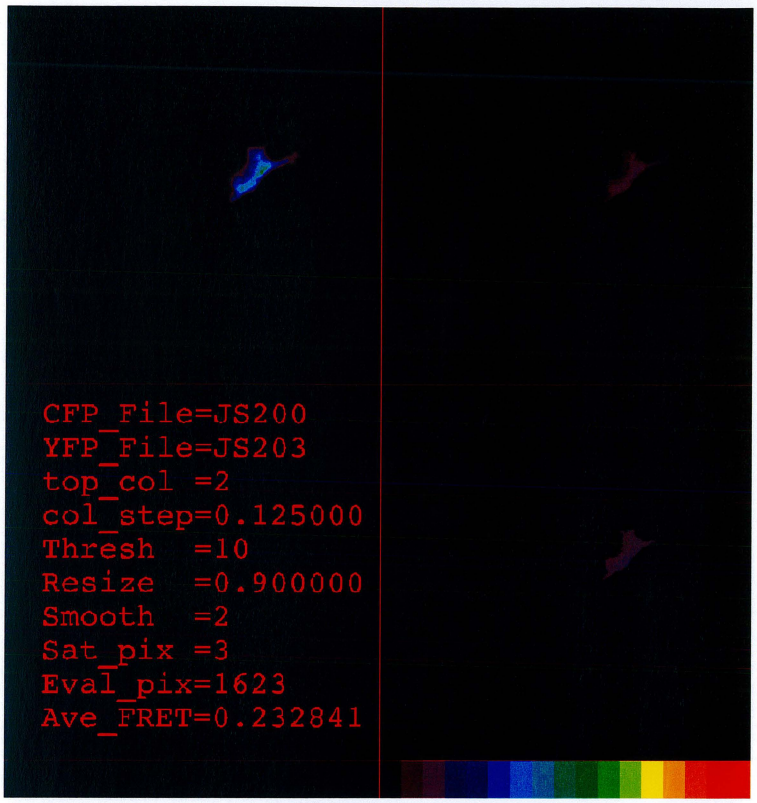

Figure 4.2.1 Steady-state on a negative ECFP control.

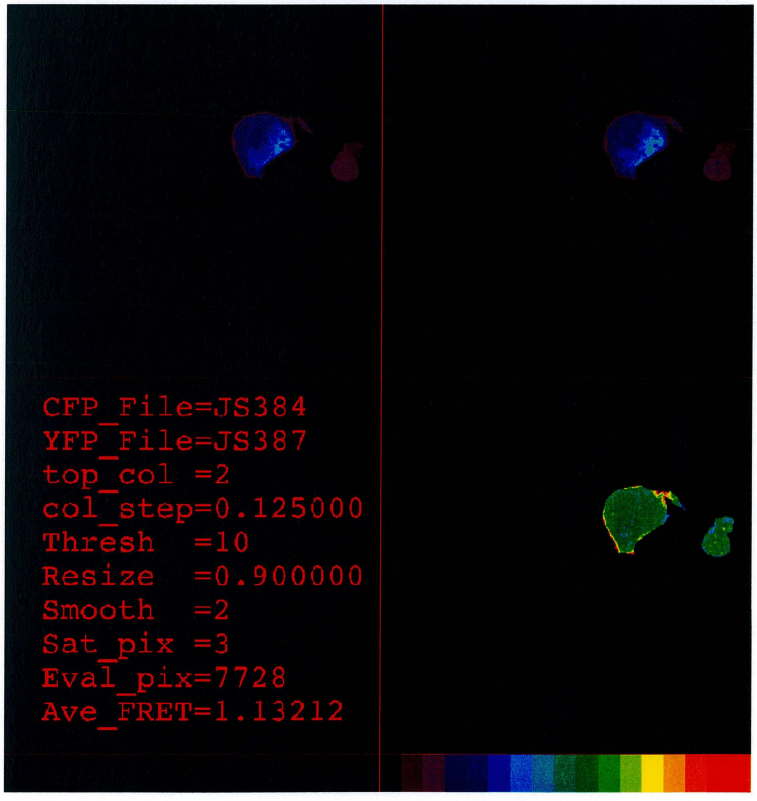

Figure 4.2.2 Steady-state on a positive control, 6aa.

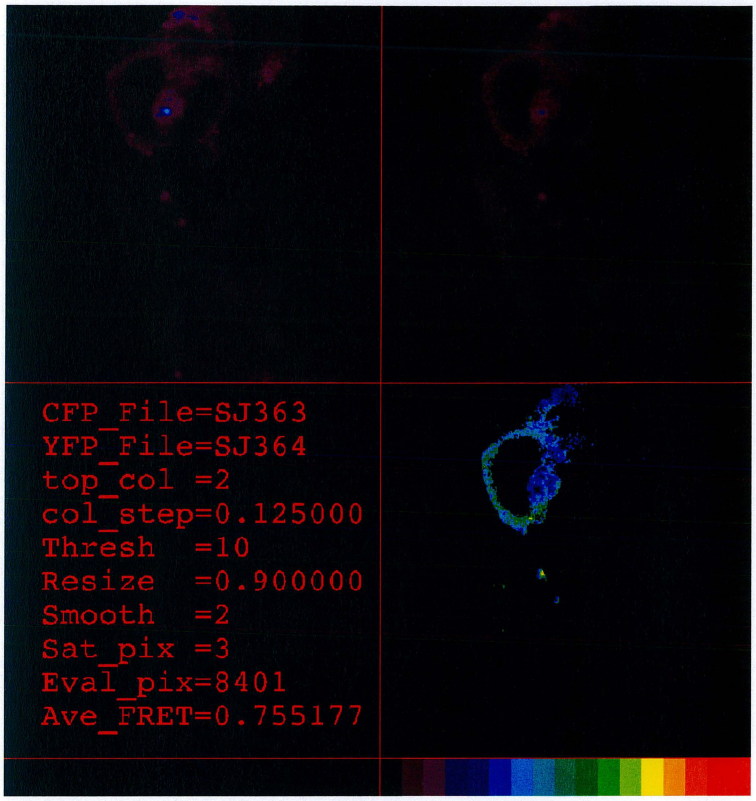

Figure 4.2.3 Steady-state on Ten-m1.

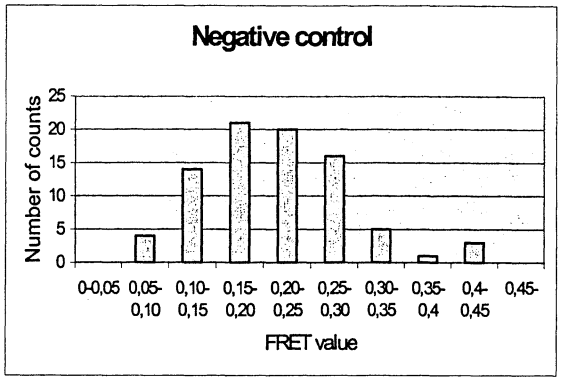

Diagram 4.2.1 Negative control

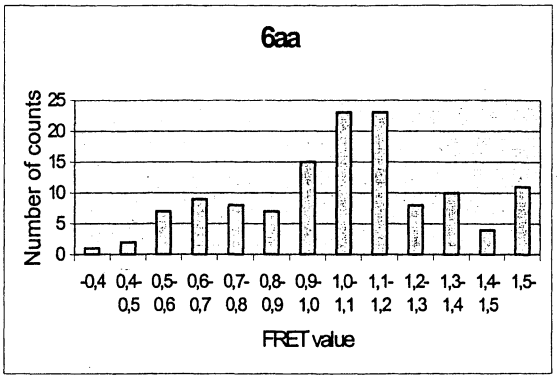

Diagram 4.2.2 Positive control 6aa

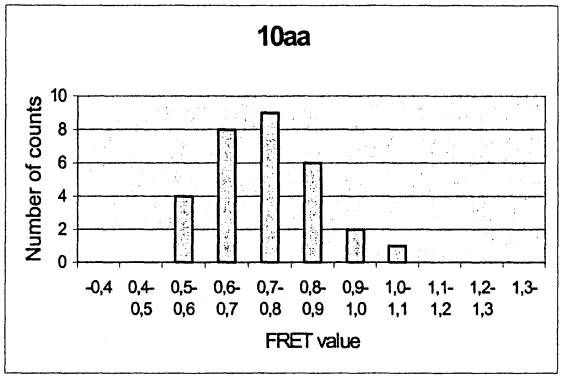

Diagram 4.2.3 Positive control 10aa

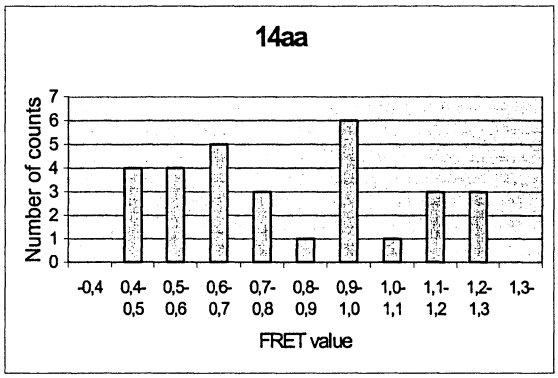

Diagram 4.2.4 Positive control 14aa

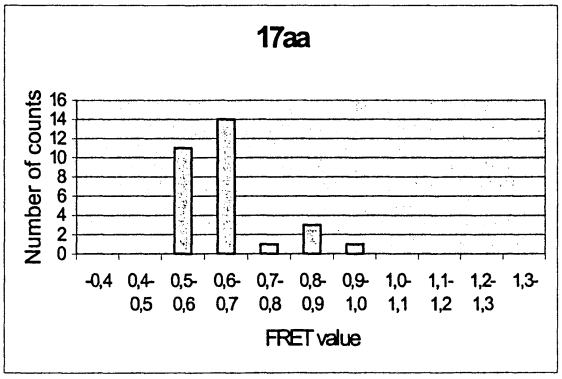

Diagram 4.2.5 Positive control 17aa

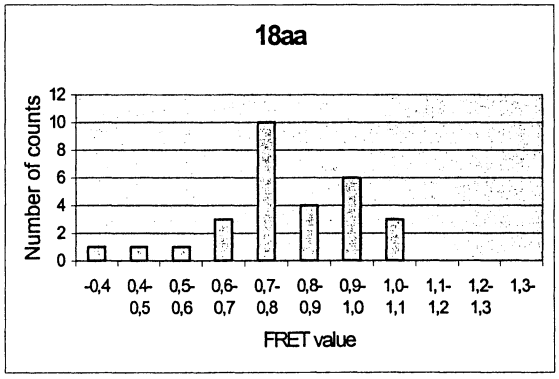

Diagram 4.2.6 Positive control 18aa

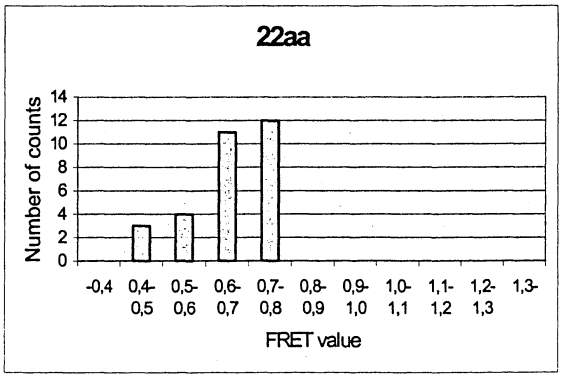

Diagram 4.2.7 Positive control 22aa

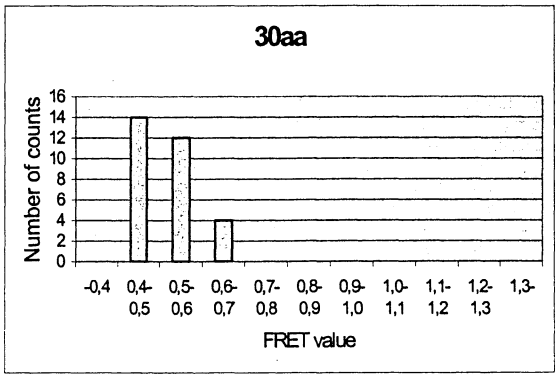

Diagram 4.2.8 Positive control 30aa

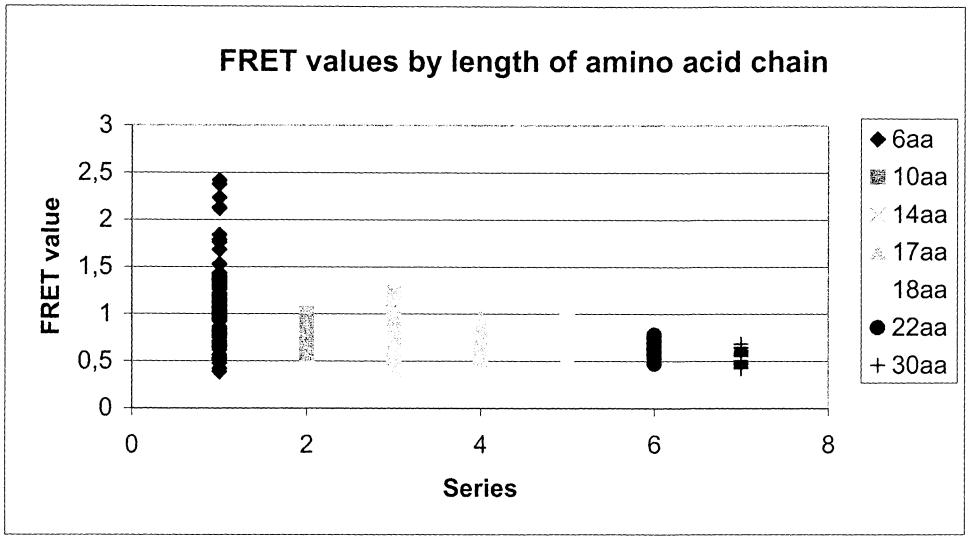

Diagram 4.2.9 Calculated FRET values by length of amino acid chain.

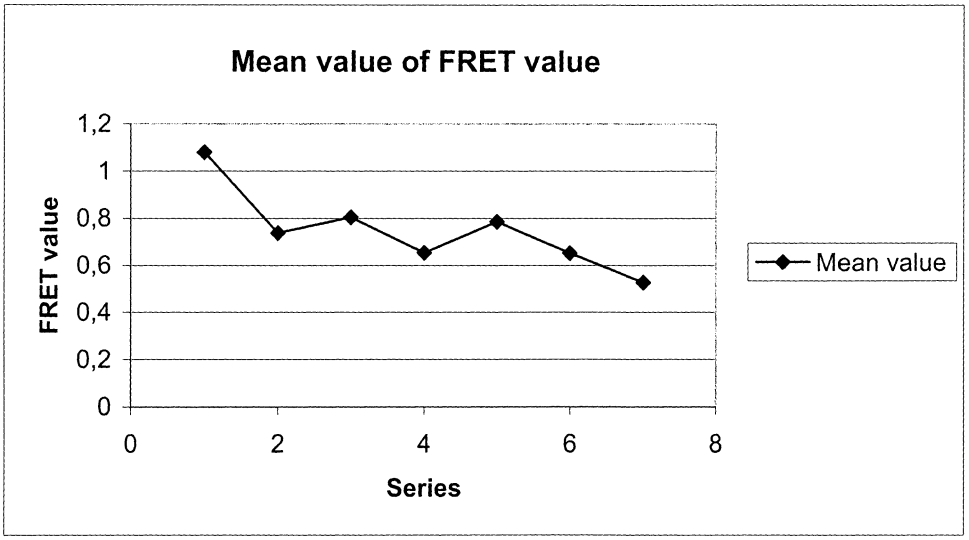

Diagram 4.2.10 Mean value of FRET values.

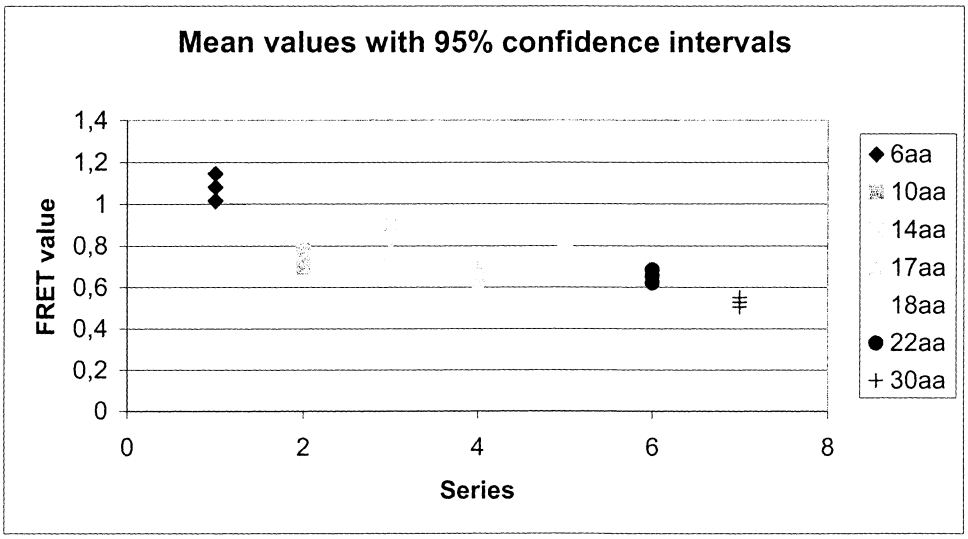

Diagram 4.2.11 Mean values of the FRET values with 95% confidence intervals

5. Discussion and conclusions

5.1 Problems

There are always properties of a measurement system, limiting its performance. For an advanced system like the one used in this study many different things can contribute to this limitation. To make it easier to discuss these properties; the system, the lasers, the samples and the methods are discussed one by one.

5.1.1 System

The set-up and the mirrors used for the Argon-ion laser beam were not optimal. First it was a very long beam path, which led to the use of a total of seven mirrors. Some of these were old and therefore had imperfections on the surface. The use of many mirrors also makes the set-up unstable and difficult to align. One other thing, which led to instability, was the mirror directing the laser beam down through the ceiling. This mirror was placed on mounting posts 15-20 cm out from the table and 1 meter above the floor that made it very sensitive to vibrations.

The first dichroic mirror in the filter box for the Argon-ion laser is suited for the Helium-Neon laser and not for this laser. This dichoic mirror led to a great loss of power. Other things that diminished the intensity were the non-linearity of the filter box. Just in front of the entrances to the filter box and the microscopic system, shutters were placed to be used in the alignment but they were not perfectly positioned. This made it impossible to use them for fine adjustments.

One of the most difficult problem to overcome in these measurements was that the alignment of the laser beams often was lost, which led to changes in the intensity into the microscope. This made it unreliable to compare the intensity in two images recorded some time apart. The reason for this possibly arose in the filter box or in the microscope, since both lasers lost their alignment in the same way at the same time and these parts of the system were the only ones they shared.

During most of the measurements there were disturbances from the renovation of the ventilation system in the laboratory. This led to vibrations and possible caused the problems experienced with misalignments.

The system used for controlling the microscope was not very stable. Sometimes the images were not saved and sometimes the software hung while scanning, which led to over-illumination of some samples. Another thing with the software was that there was only 8-bit dynamic range in the images and when performing quantitative intensity measurements a higher resolution is desirable.

5.1.2 Lasers

The Krypton-ion laser fluctuated in intensity in the beginning of the experimental part, but after optimising the laser cavity and cleaning the Brewster windows, it stabilised. This service also increased the laser power.

Since the Argon-ion laser intensity varied before reaching the right temperature, it had to warm up for about half an hour. This laser was optimized, but some fluctuations in the intensity remained, even after the warm up. The Brewster windows had to be polished once a week to avoid unwanted coatings. Such a coating could damage the laser and reduce its power.

5.1.3 Samples

There were also a few problems with the samples. The biggest one was movements of the coverslip. Because of such movements, some cells were smeared out and moved, very often outside the coverslip, which destroyed the sample.

The cells had a tendency to group themselves into clusters in the samples and this made it difficult to study single cells.

When looking at the cells with the mercury lamp, a weak blue light could be seen in the fluid surrounding the cells. This was probably some kind of auto-fluorescence.

When doing accumulations, some of the cells had a tendency to move slightly in the fluid. Such possible movement artefacts complicated the analysis.

5.1.4 Methods

Because of the fluctuations in the laser intensity, it was impossible to perform any quantitative comparisons of the intensity in two different accumulations on the same cell, no matter which one of the two methods, Bleaching or Steady-state, that was used. Except for this problem, the Steady-state measurements were relatively problem free.

The bleaching time differed somewhat from cell to cell because of the concentration variation of EYFP. Hence, to be certain that all the EYFP had been bleached, the bleaching time had to be long, as long as 15 minutes.

5.2 Conclusions

When looking at all the images taken at the laboratory sessions, it first appeared as if the FRET signal had been found and quantitatively measured. The signal from the ECFP had increased when bleaching the EYFP, and the FRET values in the Steady-state measurements were sizeable. However, after collecting all the data and analysing it, the results were no longer as easy to interpret as desired.

Going through the results from the Bleaching measurements on the positive controls, the Bleaching value was larger than 1,0 for almost every sample. This indicates that the intensity through the 470/60 nm filter has increased after bleaching. If this increase is due to a decrease of FRET, there should have been an R^{-6} dependence in the measured intensity. This dependence was, however, not observed when comparing the results from samples with different lengths in the amino acid chain. It indicates that some kind of false FRET signal was detected.

The results of the Ten-m1 sample in Fig. 4.1.4 gives, when studying it more carefully, a hint on what may cause this signal. The Ten-m1 protein marked with ECFP is clearly visible in frame 1 concentrated to the membranes in the cell as expected. The EYFP tagged profilin, on the other hand, is uniformly concentrated to the interior of the cell. After bleaching, frame 2 and frame 4 show that the intensity through the 470/60 nm filter has increased, but not in the membranes as expected, but in the interior of the cell. Since there is very little Ten-m1 protein with ECFP present in these parts of the cell, a plausible explanation is that the photoproducts created as EYFP was bleached emit blue fluorescence following violet light excitation. This is rather staggering, since the negative control specimens containing only EYFP had given no signal detectable through the 470/60 nm filter. Because of this, another control measurement was prepared only containing EYFP. Fig 5.2.1 shows the images of this control specimen.

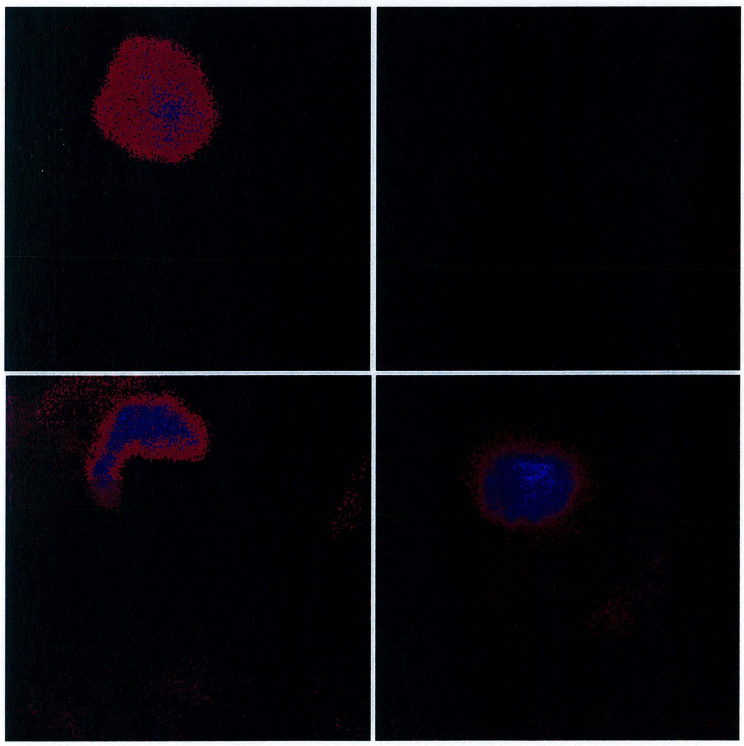

Figure 5.2.1. Images of control specimen only containing EYFP before and after bleaching.

Frame 1 shows the fluorescence of a cell excited by the 514 nm laser measured through the 540/30 nm filter. Frame 2 shows the cell following 407 nm excitation, viewed through the 470/30 nm filter. Both these images were recorded before bleaching and, as expected, there was no fluorescence in the blue spectral region from EYFP. After bleaching, frame 3 shows the cell through the 540/30 nm filter, excited with the 514 nm laser and the bleached lower right part of the cell is clearly visible.

However, when now measuring the intensity through the 470/60 nm filter, when excited with the 407 nm laser, the bleached part of the cell is fluorescing, frame 4. This means that when the EYFP is bleached, the fluorescent protein does not lose its fluorescing properties, but rather changes them. This was surprising, since it has not been seen in any literature. What actually happens to the proteins is beyond the scope of this work to explore but should be of considerable interest to other groups using EYFP in FRET measurements.

Another observation to be explained, are the three Bleaching values less than 1,0 in the results. This would mean that the intensity detected through the 470/60 nm filter decreases when the EYFP is bleached. Fig 5.2.2 shows one of these positive control cells with a Bleaching value of 0,73.

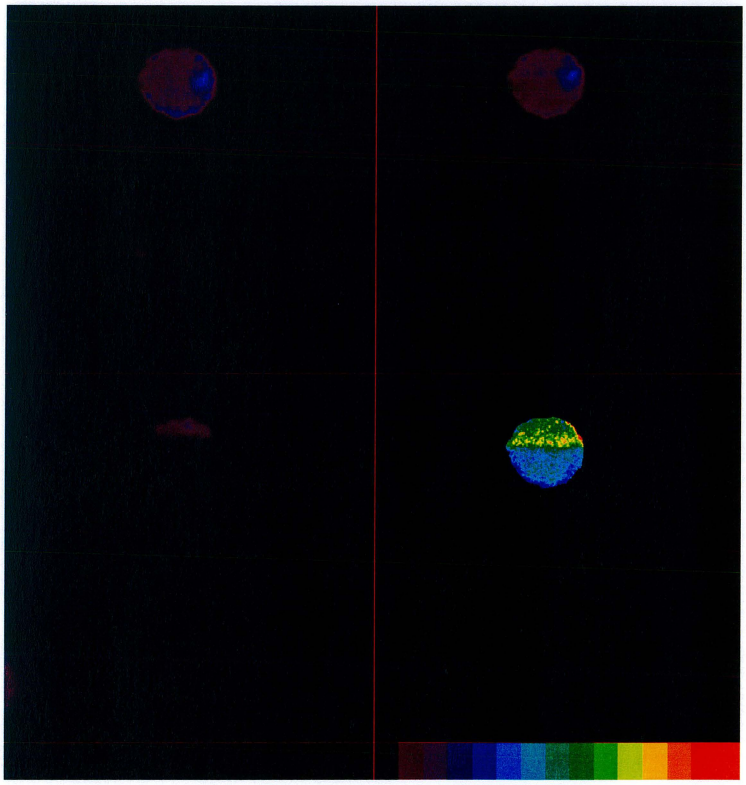

Figure 5.2.2. Images of positive control specimen with 17aa before and after bleaching.

In frames 2 and 4 it is clearly seen that the intensity has dropped in the bleached region. Negative controls have shown that the 514 nm laser used for bleaching does not affect the ECFP, and as only three cells exhibited this phenomenon, it is very difficult to draw any firm conclusions regarding this observation.

The results of the Steady-state measurements are not as discouraging concerning the interpretation of the FRET signal and the length of the amino acid chain. The negative controls exhibited a much lower average FRET value than the positive controls. The negative controls almost never have a FRET value that exceeds 0,4, while none of the positive controls had a FRET value below 0,4. There is thus a clear boundary between non-FRET and FRET signals. The high FRET values in the positive controls indicates that a large quantity of the energy is transferred to the EYFP through FRET. A R^{-6} dependence could however, not be seen.

The diagrams 4.2.1-4.1.8 shows a clear decrease in FRET value with increasing length in the amino acid chain, but the decrease is not sufficiently large. This may be interpreted as an uncertainty in the distance between the ECFP and the EYFP in the samples. If the concentration of fluorochromes is too high, the average distance between neighbouring proteins could be less than the length of the amino acid chain.

Another explanation of the results could be a folding of the amino acid chains. There is no guarantee that the chain will stay "straight" when linking two fluorescent proteins built of hundreds of amino acids. Such a folding would ruin every attempt to measure the distance between the two proteins. The structure and the individual amino acids in the chain also contribute to the folding. Certain amino acids have a tendency of introducing "curves" on the chain. For example the 18aa chain is built with a slightly different structure than the 17aa chain, which could induce folding more often. This could explain the higher FRET values on the 18aa sample. This kind of folding can possibly also explain the higher standard deviation of the mean value of the 10aa sample. Another aspect of FRET is the effect of the orientation of the proteins on the signal. When linking them to an amino acid chain, it is very difficult to predict how they will orient themselves to each other.

These effects probably contributed to the results in this work. The FRET values measured for the positive controls are mean values through out the cells and reflect the average distance between two fluorescent proteins. Some of the amino acid chains are probably unaffected by the effects discussed above, which is why the average value of the intensity still shows a decrease with amino acid chain length. However, the uncertainties in the evaluation of distance between the two proteins seem too large for this method to provide information of interest for any application. It is also probable that the effects described above are dependent on the microenvironment in the cell and no positive results could be made from the control specimens to use as reference to the Ten-m1 samples.

5.3 The Future

Since the FRET method seems to be a very good method for measuring the reactions in living cells, it is very important to develop and improve it.

To make the bleaching process work, one suggestion is to use another fluorescent protein pair. One of them can perhaps be the new protein that fluoresces in red, called DsRed. One other thing that should simplify the bleaching is to find some fluorescent protein that has shorter bleaching time, but not too short so that it is bleached while doing accumulations. The Steady-state method can probably be improved by using three sets of filters as described in chapter 2.5.2. This has the advantage of direct acquisition of images of different PMTs, which can make the FRET measurements more accurate.

To be able to see the R^{-6} dependence of the FRET signal in the control samples, folding must be avoided. One suggestion to achieve this is to make the positive controls in another way than the way they are made now. This could be done, for instance, by using a membrane with known thickness and a transmembrane protein instead of the amino acid chain. The transmembrane protein could then be marked with two different fluorescent proteins at different sides of the membrane. This will make the folding impossible and the distance between the two fluorochromes will be well-known.

An advanced system like the one used for the experiments can always be improved and made more sensitive, to make the measurements easier and better. For example the resolution, which is only 8-bit, should be increased.

The change in EYFP fluorescence properties after bleaching has to be further investigated. It also has to be compared with results presented in other papers that have used this fluorochrome, to find out if they have experienced the same problems. This discovery also may be useful in other experiments such as diffusion measurements i.e. by bleaching just a small area of a cell only containing EYFP and then observe how the proteins with altered fluorescence properties move during a certain time period. It can also be improved to a two-way diffusion measurement simply by changing detection filter and also observe how the unbleached proteins move into the bleached area.

6. Acknowledgements

We would like to thank a few people for the help to make this diploma paper.
First, we want to thank Clemens Kaminski and Stefan Andersson-Engels for guiding us throughout this work.

We would also want to thank Dr. Hui Zhang and Dr. Uwe Rauch at the Department of Experimental Pathology at Lund University Hospital for the cell samples received and used in our experiments.

Finally, we want to thank everybody at the Department of Atomic Physics and especially Tommy Sjögren and Claes af Klinteberg for all their help.

7. References

1. X. F. Wang, B. Herman (eds.), *Fluorescence Imaging Spectroscopy and Microscopy*, John Wiley & Sons, Inc., 1996.

2. A. K. Kirsch, V. Subramaniam, A. Jenei, T. M. Jovin, "Fluorescence Resonance Energy Transfer Detected by Scanning Near-field Optical Microscopy", *Journal of Microscopy*, Vol. 194, p. 448-454, May/June 1999.

3. G. W. Gordon, G. Berry, X. H. Liang, B. Herman, "Quantitative Fluorescence Resonance Energy Transfer Measurements Using Fluorescence Microscopy", *Biophysical Journal*, Vol.74, p. 2702-2713, May 1998.

4. B. A. Herman, S. M. Fernandez, "Dynamics and Topographical Distribution of Surface Glycoproteins during Myoblast Fusion: A Resonance Energy Transfer Study", *Biochemistry*, Vol 21, p. 3275-3283, 1982.

5. T. Förster, "Energiewanderung und Fluoreszenz", *Die Naturwissenschaften*, Heft 6, p. 166-175, 1946.

6. P. S. Uster, R. E. Pagano, "Resonance Energy Transfer Microscopy: Observations of Membrane-bound Fluorescent Probes in Model Membranes and in Living Cells", *The Journal of Cell Biology*, Vol 103, p.1221-1234, October 1986.

7. S. A. Vickery, R. C. Dunn, "Scanning Near-Field Fluorescence Resonance Energy Transfer Microscopy", *Biophysical Journal*, Vol 76, p. 1812-1817, April 1999

8. O. J. Rolinski, D. J. S. Birch, L. J. McCartney, J. C. Pickup, "A Method of determining donor-acceptor distribution functions in Förster resonance energy transfer", *Chemical Physics Letters*, Vol 324, p. 95-100, 2000.

9. *Fluorescence Resonance Energy Transfer spectroscopy*, http://www.anatomy.usyd.edu.au/mru/fret/abot.html

10. N. P. Mahajan, K. Linder, G. Berry, G. W. Gordon, R. Heim, B. Herman, "Bcl-2 and Bax interactions in mitochondria probed with green fluorescent protein and fluorescence resonance energy transfer", *Nature Biotechnology*, Vol 16, p. 547-552, June 1998.

11. T. Oohashi, X-H. Zhou, K. Feng, B. Richter, M. Mörgelin, M. T. Perez, W-D. Su, R. Chiquet-Ehrismann, U. Rauch, R. Fässler, "Mouse Ten-m/Odz Is a New Family of Dimeric Type II Transmembrane Proteins Expressed in Many Tissues", *The Journal of Cell Biology*, Vol 145(3), p. 563-577, 1999.

12. H. Bayley, "Building Doors into the cells", *Scientific American*, p42-47, September 1997.

13. S. Svanberg, *Atomic and Molecular Spectroscopy*, Springer-Verlag, 2nd ed., 1992.

14. CLONTECH Laboratories, Inc., *Living Colors User Manual*, April 1999.

15. *Living Colors*, http://www.clontech.com

16. B. Alberts, D. Bray, J. Lewis, M. Raff, K. Roberts, J. D. Watson, *Molecular Biology of the Cell*, Garland Publishing, Inc., 3rd ed., 1994.

17. A. J. F. Griffiths, J. H. Miller, D. T. Suzuki, R. C. Lewontin, W. M. Gelbart, *An Introduction to Genetic Analysis*, W. H. Freeman and Company, 5th ed., 1993.

18. J. S. Cohen, M. E. Hogan, "The new Genetic Medicines", *Scientific American*, p. 50-55, December 1994.

19. O. Svelto, *Principles of Lasers*, Plenum Press, 4th ed., 1998.

20. J. B. Pawley, *Handbook of Biological Confocal Microscopy*, Plenum Press, 2nd ed., 1995.

21 J. W. Lichtman, "Confocal Microscopy", *Scientific American*, p. 30-35, August 1994.

22. BIO-RAD Microscopy Division, *MRC-1024 Laser Scanning Confocal Imaging System: User Operating Manual*, May 1996.

23. S-G. Pettersson, S. Borgström, H. Hertz, *Advanced Optics*, Department of Physics, LTH, 1999.

Appendix

```
pro call_Fret_Analysis2


INpath='C:\bilderpic\'
OUTpath='results\' ;

CFP_file='JS859.PIC' ;470/60 filter
YFP_file='JS861.PIC' ;540/30 filter
Bleach_File='JS860.PIC'
;PIC_file='JS856.PIC'
I_Biorad=1      ;TRUE: read in PIC format direct,
                ;FALSE: read in TIFF format

smooth_para=2    ; degree of smoothing before division
threshold=5  ; minimum signal to be considered for calculations
topscale=7.0      ; largest FRET ratio expected (=TOPCOLOUR!)
Colour_Units=0.125 ;this allows to specify what distance ther is between different colours
Final_Resize=0.9 ;reduce size of final image by this factor!

i=FRET_Analysis2(InPath, OutPath, CFP_File,  $
   YFP_File, Bleach_File, Smooth_para, threshold, topscale, $
   Final_Resize, Colour_Units, I_Biorad)

;i=import_Biorad(InPath, PIC_file)
;write_multi_pics, i, PIC_file, outpath, gif ; this writes the result as a gif
                                ;image in the directory specified
                                ;INPATH + OUTPATH
end


function FRET_Analysis2, InPath, OutPath, CFP_File, $
      YFP_File, Bleach_File, Smooth_para, threshold, topscale, $
      Final_Resize, Colour_Units, I_Biorad
DEVICE, RETAIN=2, DECOMPOSED=0


;---------  read files in ----------

if (I_Biorad eq 0) then begin

complete_file=InPath+YFP_file
CFP = READ_TIFF(complete_file)
complete_file=InPath+YFP_file
YFP = READ_TIFF(complete_file)

endif else begin

CFP = IMPORT_BIORAD(InPath, CFP_File)
YFP = IMPORT_BIORAD(InPath, YFP_File)
BLEACH=IMPORT_BIORAD(InPath, Bleach_File)
endelse

;--------  smooth files ----------
if (smooth_para gt 1) then begin
CFP=smooth(CFP, smooth_para)
YFP=smooth(YFP, smooth_para)
endif

CFP_size=size(CFP)




;------- FRET Pictures ---------

;  exclude regions that are saturated and not zero:
   region = where(((cfp LT 255) AND (yfp LT 255)) $
```

```
70              AND ((cfp GT threshold) AND (yfp GT threshold)), Countem)
        sat_reg=where((cfp EQ 255) OR (yfp EQ 255))
        sat_reg=size(sat_reg)

    ;  divide pictures where above is satisfied
75      FRET=Make_Array(CFP_size[1], CFP_size[2], /FLOAT, Value=0.0)

    If countem NE 0 then begin
        FRET[region]=FLOAT(YFP[region])/FLOAT(CFP[region])

80      Print, 'maxFret=', max(FRET)
        FretVector=FRET[region]
        FRETCOUNT=FRET
        FRET=ROUND(ROUND(255*(FRET/(TOPSCALE*Colour_Units)))*Colour_Units)
    ENDIF
85      FRET=Byte(FRET)
        Mean_fret=mean(fretVector)
        print, 'Meanfret_Signal=', Mean_fret
        evaluated_pixels=size(region)
        print, 'number of evaluated pixels=', evaluated_pixels[1]
90  ;----- show only pixels higher than cfp FRET ratio
        CFP_Fret_ratio=0.0
        region_1=where(fretVector GT CFP_FRET_RATIO)
        Mean_fret=mean(fretVector[region_1])
        print, 'Meanfret_Signal>cfp=', Mean_fret
95      evaluated_pixels=size(region_1)
        print, 'number of evaluated pixels>CFP_FRET_Ratio=', evaluated_pixels[1]

    ;----- produce colour LUT scales -----
        LUT=topscale/Colour_Units*(Findgen(CFP_size[1])/Float(CFP_size[1]))
100     scale=(LUT#transpose(replicate(1, 50)))
        ;scale=byte(round(255*scale/12))
        scale=bytscl(scale, max=topscale/Colour_Units, top=topscale/Colour_Units)
        scale=bytscl(scale)

105 ;------ preparing for text output! ------
    x=cfp_size[1]-3
    y=cfp_size[2]-3
    u=make_array(x, y, /BYTE, VAlUE=0)

110
    CFP_file_ex=STRSPLIT(CFP_file, '.', /EXTRACT)
    YFP_file_ex=STRSPLIT(YFP_file, '.', /EXTRACT)

    cfp_f='CFP_File='+cfp_file_ex[0]
115 yfp_f='YFP_File='+yfp_file_ex[0]
    top=  'top_col ='+strcompress(string(FIX(topscale)), /remove_All)
    col=  'col_step='+strcompress(string(colour_units), /remove_All)
    thr=  'Thresh  ='+strcompress(string(threshold), /remove_All)
    res=  'Resize  ='+strcompress(string(Final_Resize), /remove_All)
120 smo=  'Smooth  ='+strcompress(string(smooth_para), /remove_All)
    sat=  'Sat_pix ='+strcompress(string(sat_reg[1]), /remove_All)
    eva=  'Eval_pix='+strcompress(string(evaluated_pixels[1]), /remove_All)
    fre=  'Ave_FRET='+strcompress(string(Mean_Fret), /remove_All)

125 vec=[cfp_f, yfp_f, top, col, thr, res, smo, sat, eva, fre]
    ves=size(vec)
    sx=round(x/10)
    sy=round(y/(ves[1]+1))
    yst=REVERSE((bindgen(ves[1])+1)*sy)
130 XST=REPLICATE(SX, ves[1])

    ;display_array, u, 1, 'TEXT!'
    DEVICE, FONT='Courier', /TT_FONT, SET_CHARACTER_SIZE=[25,28]
    XYOUTS, XST, YST, vec, FONT=1, /DEVICE
135 TEXT=TVRD()       ;read the window and store it!
    wdelete

    ;----- put everything into one massive picture -----
```

```
    y=make_array(cfp_size[1]*2, cfp_size[2]*2+50, /byte)
140 y_size=size(y)

    y[cfp_size[1]*1,cfp_size[2]*0]=[scale]
    y[cfp_size[1]*0,cfp_size[2]*0+50]=BLEACH
    y[cfp_size[1]*1,cfp_size[2]*0+50]=FRET
145 y[cfp_size[1]*0,cfp_size[2]*1+50]=cfp
    y[cfp_size[1]*1,cfp_size[2]*1+50]=yfp
    ;---- chops pic into 4 segments
    y[cfp_size[1]:cfp_size[1]+1,*]=255
    y[*, cfp_size[2]+50:cfp_size[2]+51]=255
150 y[*,50:51]=255
    y=congrid(y, ROUND(y_size[1]* Final_Resize), $
       ROUND(y_size[2]* Final_Resize))

    ;----- display whatever you want to display -----
155 ;display_array, u_CFP, 0, 'CFP '+CFP_file
    ;display_array, u_YFP, 1, 'YFP '+YFP_file
    ;display_array, FRET, 3, 'FRET'+YFP_file+'/'+CFP_file
    ;display_array, scale, 4, 'scale'
    display_array, y, 0, 'EVERYTHING'
160   ;-------Calculate the fret signal in one region----------
    ;print, 'Välj ut ett område som inte blekts'
    ;box_cursor, x1, y1, x2, y2
    ;compreg1=make_array(x2, y2)
    ;compreg1_size=size(copmreg1)
165 ;compreg1=FRETCOUNT[x1:(x1+x2), y1:(y1+y2)]
    ;compmean1=mean(compreg1)
    ;print, 'FRET1=', compmean1
     ;------Calculate the Fret signal in another region and calculate the fret quote-----
    ;print, 'Välj ut ett område som har blekts'
170 ;box_cursor, x1, y1, x2, y2
    ;compreg2=make_array(x2, y2)
    ;compreg2_size=size(compreg2)
    ;compreg2=FRETCOUNT[x1:(x1+x2), y1:(y1+y2)]
    ;compmean2=mean(compreg2)
175 ;print, 'FRET2=', compmean2
    ;Fret_quote=compmean2/compmean1
    ;print, 'FRET_QUOTE=', Fret_quote

    tvlct, R, G, B, /GET
180
    goto, jump2

    ;------ conditional file_write ------------
    print, 'write to file (Y/N)? '
185    A = GET_KBRD(1)
       PRINT, A

       if A EQ 'y' then begin

190       out=INPath+OUTpath+CFP_File_ex+'_i.gif'
          write_gif, out, i, R, G, B

          ;outpath=path+outdir+file_ex[0]+'_i1.gif'
          ;write_gif, outpath, i1, R, G, B
195       ;outpath=path+outdir+file_ex[0]+'_i2.gif'
          ;write_gif, outpath, i2, R, G, B
          ;outpath=path+outdir+file_ex[0]+'_i3.gif'
          ;write_gif, outpath, i3, R, G, B
       endif
200 ;------- file out
    jump2:

    out=INPath+OUTpath+CFP_File_ex[0]+YFP_File_ex[0]+'_fret.gif'
    write_gif, out, y, R, G, B
205
    v=1
    return, v
```

```
    end

pro box_cursor, x0, y0, nx, ny, INIT = init, FIXED_SIZE = fixed_size, $
   MESSAGE = message

   DEVICE, GET_GRAPHICS = old, SET_GRAPHICS = 6  ;Set xor
   col = !D.N_COLORS -1
   corner = 0

   if KEYWORD_SET(message) then begin
      print, "Drag Left button to move box."
      print, "Drag Middle button near a corner to resize box."
      print, "Right button when done."
   endif

   if KEYWORD_SET(init) eq 0 then begin ;Supply default values for box:
      if KEYWORD_SET(fixed_size) eq 0 then begin
         nx = !D.X_SIZE/8    ;no fixed size.
         ny = !D.X_SIZE/8
      endif
      x0 = !D.X_SIZE/2 - nx/2
      y0 = !D.Y_SIZE/2 - ny/2
   endif

   button = 0
   old_button = 1
   goto, middle

   while(1) do begin
      old_button = button
      cursor, x, y, 2, /DEV   ;Wait for a button
      button = !MOUSE.BUTTON

      if ((old_button eq 0) and (button ne 0)) then begin
         mx0 = x     ;For dragging, mouse locn...
         my0 = y
         x00 = x0          ;Orig start of ll corner
         y00 = y0
      endif

      if (!MOUSE.BUTTON eq 1) then begin ;Drag entire box?
         x0 = x00 + x - mx0
         y0 = y00 + y - my0
      endif

      ;;New size?
      if ((!MOUSE.BUTTON eq 2) and (KEYWORD_SET(fixed_size) eq 0)) $
       then begin
         if (old_button eq 0) then begin ;Find closest corner
            mind = 1e6
            for i=0,3 do begin
               d = float(px[i]-x)^2 + float(py[i]-y)^2
               if (d lt mind) then begin
                  mind = d
                  corner = i
               endif
            endfor
            nx0 = nx    ;Save sizes.
            ny0 = ny
         endif
         dx = x - mx0 & dy = y - my0 ;Distance dragged...
         case corner of
            0: begin
               x0 = x00 + dx & y0 = y00 + dy
               nx = nx0 -dx & ny = ny0 - dy
            endcase
            1: begin
               y0 = y00 + dy
               nx = nx0 + dx & ny = ny0 - dy
```

```
                endcase
                2: begin
                   nx = nx0 + dx & ny = ny0 + dy
280             endcase
                3: begin
                   x0 = x00 + dx
                   nx = nx0 -  dx & ny = ny0 + dy
                endcase
285          endcase
          endif

          if ((old_button ne 0) or (button ne 0)) then begin
             plots, px, py, COL=col, /DEV, THICK=1, LINES=0 ;Erase previous box
290          empty                ;Decwindow bug
       endif

          if (!MOUSE.BUTTON eq 4) then begin ;Quitting?
             DEVICE,SET_GRAPHICS = old
295          return
          endif
       middle:

          if (nx lt 0) then begin
300          x0 = x0 + nx
             nx = -nx
          case corner of
          0: corner = 1
          1: corner = 0
305       2: corner = 3
          3: corner = 2
          endcase
       ; reset the starting drag point...
             mx0 = x & my0 = y
310          x00 = x0 & y00 = y0
             nx0 = nx & ny0 = ny
          endif
          if (ny lt 0) then begin
             y0 = y0 + ny
315          ny = -ny
          case corner of
          0: corner = 3
          3: corner = 0
          1: corner = 2
320       2: corner = 1
          endcase
       ; reset the starting drag point...
             mx0 = x & my0 = y
             x00 = x0 & y00 = y0
325          nx0 = nx & ny0 = ny
          endif

          x0 = x0 > 0
          y0 = y0 > 0
330       x0 = x0 < (!D.X_SIZE-1 - nx) ;Never outside window
          y0 = y0 < (!D.Y_SIZE-1 - ny)

          px = [x0, x0 + nx, x0 + nx, x0, x0] ;X points
          py = [y0, y0, y0 + ny, y0 + ny, y0] ;Y values
335
          if ((old_button ne 0) or (button ne 0)) then begin
             plots,px, py, COL=col, /DEV, THICK=1, LINES=0 ;Draw the box
             empty                ;Decwindow bug
       endif
340
          wait, .1       ;Dont hog it all
       endwhile
    end

345 pro display_array, image, WindowNumber, WindowTitle
```

```
;+++++++++++++++++++++++++++++++++++++++++++++++++++++++
;program that displays images in different windows
;+++++++++++++++++++++++++++++++++++++++++++++++++++++++
image_size=Size(image)
image_size=reform(image_size[1:2])
window, WindowNumber, xsize=image_size[0], ysize=image_size[1], title=WindowTitle
TVSCL, image
;profiles, image
end

function import_Biorad, InPath, PIC_file

file=InPath+PIC_file
i=Read_Binary(file, Data_Start=0, Data_DIMS=76)

X_Size=i[0]+256*i[1]  ; Size of pics in x
Y_Size=i[2]+256*i[3]  ; Size of pics in y
NPICS=i[4]+256*i[5]   ; Number of pics stored in File
;NPICS=1

for counter=0, 75, 1 Do Begin
print,'counter=',counter,':', i[counter]
;print,'counter=',counter,':', i[counter]+i[counter+1]*256
endfor


print, 'X_Size:', X_Size
print, 'Y_Size:', Y_Size
print, 'NPICS:', NPICS

i=READ_BINARY (file, DATA_START=76, DATA_DIMS=[X_Size,Y_Size,NPICS])
;i=REFORM(i)
help, i
for counter=1, NPICS-1 do begin
display_array, i[*,*,counter], 0, file
;wait,0.5
endfor
return,i


end

pro resize_image, InPath, OutPath, FlameArea
;?++++++++++++++++++++++++++++++
;+Program that changes the image size to interesting regions
;given in FlameArea
;e.g. FlameArea=[200,480,10,374];x1,x2,y1,y2
;Processes all files in InPath
;CFK 19 March 2000
;++++++++++++++++++++++++++++++
;
;FlameArea=[200,480,10,374];x1,x2,y1,y2
;InPath='C:\Science\LLC2_Processed\PM\'
;OutPath='C:\Science\LLC2_Processed\PM\Final\'


xlength=FlameArea[1]-FlameArea[0]+1
ylength=FlameArea[3]-FlameArea[2]+1
InVector=comp_dir(InPath, OutPath)
print, invector
;stop, invector
InSize=Size(InVector)
print,'########################'
for counter=0, InSize(1)-1 DO BEGIN
;for counter=0, 1 DO BEGIN
   print, InVector[counter]
   i=load_gif(InVEctor[counter])
   display_array, i, 0, 'resize_1'
   ;rdpix, i
```

```
415       FlameImage=Make_Array((FlameArea[1]-FlameArea[0]+1),(FlameArea[3]-FlameArea[2]+1),8,/FLOAT)
          FlameImage=i[FlameArea[0]:FlameArea[1],FlameArea[2]:FlameArea[3]]
          display_array, FlameImage, 2, 'resize_1'
          OutName=OutPath+sep_FileName(InVector[counter])
          write_gif, OutName, Flameimage
420
       endfor
       end

       function split_file_name, inName
425    OutFilePath='C:\Clemens\papers\Bai_Xusong_1\Data\Out\'
       ;++++++++++++++++++++++++++++++++
       ; SEPARATES OUT bits in a FILENAME
       ; COMPLETE PATH NAME
       ;++++++++++++++++++++++++++++++++
430
          FileName=strsplit(inName, '.', /extract)    ;THIS COMMAND SPLITS INVECTOR INTO THE BITS BEWTWEEN
          ;print, FileName                                    ;'\'s
          Dummy=Size(Filename)
          ;File=Filename[Dummy[1]-2]+'.'+Filename[Dummy[1]-1] ; keeps last two parts in name
435       ;stop, File
          File=FileName
       return, File
       End

440    pro write_multi_pics, images, filename, outpath, type
       ;*****************************************
       ;*  PROGRAM TO EXPORT A LARGE ARRAY INTO *
       ;*    SEVERAL FORMATS                    *
       ;*****************************************
445
       ;+++++ check dimensions of input array
       Image_dims=size(images)
       x_dims=Image_dims[1]
       Y_dims=Image_dims[2]
450    Num_pics=Image_dims[3]
       print, Image_dims

       ;+++++ write out images
       ;print, outpath
455    for counter=0, Num_PICS-1 do begin
          file=split_file_name(filename)
          if (counter LT 10) then begin
          file=outpath+file[0]+'_0'+strcompress(string(counter), /Remove_all)+'.gif'
          endif else begin
460       file=outpath+file[0]+'_'+strcompress(string(counter), /Remove_all)+'.gif'
          endelse
          print, file
          write_gif, file, images[*,*, counter]
       endfor
465
       end
```